

## RESEARCH

# A xenograft and cell line model of SDH-deficient pheochromocytoma derived from *Sdhb*<sup>+/-</sup> rats

James F Powers<sup>1</sup>, Brent Cochran<sup>2</sup>, James D Baleja<sup>2</sup>, Hadley D Sikes<sup>3</sup>, Andrew D Pattison<sup>4</sup>, Xue Zhang<sup>2</sup>, Inna Lomakin<sup>1</sup>, Annette Shepard-Barry<sup>1</sup>, Karel Pacak<sup>5</sup>, Sun Jin Moon<sup>3</sup>, Troy F Langford<sup>3</sup>, Kassi Taylor Stein<sup>3</sup>, Richard W Tothill<sup>4,6</sup>, Yingbin Ouyang<sup>7</sup> and Arthur S Tischler<sup>1</sup>

<sup>1</sup>Department of Pathology and Laboratory Medicine, Tufts Medical Center, Tufts University School of Medicine, Boston, Massachusetts, USA

<sup>2</sup>Department of Developmental, Molecular and Chemical Biology, Tufts University School of Medicine, Boston, Massachusetts, USA

<sup>3</sup>Department of Chemical Engineering, Massachusetts Institute of Technology, Cambridge, Massachusetts, USA

<sup>4</sup>Department of Clinical Pathology, University of Melbourne, Melbourne, Victoria, Australia

<sup>5</sup>Section on Medical Neuroendocrinology, Eunice Kennedy Shriver Division National Institute of Child Health and Human Development, Bethesda, Maryland, USA

<sup>6</sup>Peter MacCallum Cancer Centre, Melbourne, Victoria, Australia

<sup>7</sup>Cyagen US Inc, Santa Clara, California, USA

Correspondence should be addressed to J F Powers: [jpowers1@tuftsmedicalcenter.org](mailto:jpowers1@tuftsmedicalcenter.org)

## Abstract

Tumors caused by loss-of-function mutations in genes encoding TCA cycle enzymes have been recently discovered and are now of great interest. Mutations in succinate dehydrogenase (SDH) subunits cause pheochromocytoma/paranglioma (PCPG) and syndromically associated tumors, which differ phenotypically and clinically from more common SDH-intact tumors of the same types. Consequences of SDH deficiency include rewired metabolism, pseudohypoxic signaling and altered redox balance. PCPG with *SDHB* mutations are particularly aggressive, and development of treatments has been hampered by lack of valid experimental models. Attempts to develop mouse models have been unsuccessful. Using a new strategy, we developed a xenograft and cell line model of SDH-deficient pheochromocytoma from rats with a heterozygous germline *Sdhb* mutation. The genome, transcriptome and metabolome of this model, called RS0, closely resemble those of *SDHB*-mutated human PCPGs, making it the most valid model now available. Strategies employed to develop RS0 may be broadly applicable to other SDH-deficient tumors.

## Key Words

- ▶ succinate dehydrogenase B
- ▶ paranglioma
- ▶ pheochromocytoma
- ▶ cluster 1
- ▶ xenograft
- ▶ cell culture
- ▶ hypoxia
- ▶ metabolome
- ▶ model
- ▶ rat

Endocrine-Related Cancer  
(2020) 27, 337–354

## Introduction

Paranglia are neuroendocrine structures that develop from neural crest progenitors associated with paraxial sympathetic nerves and from parasympathetic nerves in the head and neck. The major sympathetic paranglion is the adrenal medulla. Tumors called parangliomas can arise anywhere in the distribution of normal paranglia. By definition an intra-adrenal paranglioma (PG) is called a pheochromocytoma (PC) (Lloyd *et al.* 2017).

At least 40% of pheochromocytomas and parangliomas (PCPGs) are hereditary, and germline mutations of at least 17 functionally diverse genes can lead to their development (Dahia 2017). Mutations of genes encoding subunits of succinate dehydrogenase (SDH) account for the largest number of familial aggregates of these tumors and for more than 20–30% of the tumors that metastasize (Amar *et al.* 2005, 2007, Benn *et al.* 2006,

Pasini & Stratakis 2009, Favier *et al.* 2015). Mutations of *SDHB*, which encodes the B subunit, confer the highest risk of metastasis (Crona *et al.* 2019, Hescot *et al.* 2019). Specifically, about 42% of *SDHB* mutation carriers develop pheochromocytomas or paragangliomas by the age of 70 (Jochmanova *et al.* 2017, Rijken *et al.* 2017), and up to almost 60% of the tumors have been reported to metastasize (Jochmanova *et al.* 2017). There is currently no cure after metastases occur. Further, there are few experimental models for pre-clinical testing of new treatments and no models that faithfully reflect the tumor phenotype.

Paragangliomas sort into clusters based on their transcriptome and associated phenotypic characteristics, which include signaling pathways, metabolism and hormonal function (Dahia *et al.* 2005, Richter *et al.* 2014, Castro-Vega *et al.* 2015, Favier *et al.* 2015, Fishbein *et al.* 2017, Fishbein & Wilkerson 2018). Tumors with gene mutations of SDH subunits fall into cluster 1, which is characterized by pseudohypoxic signaling and metabolism (Eisenhofer *et al.* 2017). In contrast, cluster 2, the second major aggregate of tumors, is associated predominantly with mutations of genes including *RET* and *NF1* that affect kinase signaling. It is important for pre-clinical models to represent the appropriate tumor cluster as closely as possible because distinctive cluster-associated signaling and metabolic (Richter *et al.* 2014, Lussey-Lepoutre *et al.* 2015) characteristics can potentially serve as drug targets (Tella *et al.* 2017) or modify drug responses (Muir & Vander Heiden 2018). However, genetically engineered mice with *Sdhb* mutations have thus far failed to develop SDH-deficient PCPGs. Consequently, cluster 2 mouse tumor models are often used as imperfect surrogates (Lussey-Lepoutre *et al.* 2018).

In contrast to mice and other species, rats have an unusual proclivity to develop PCs. The incidence of these tumors increases throughout life and is especially high in males compared to females, with a ratio up to 10:1 in some rat strains (Tischler *et al.* 2014). Abdominal or head and neck PGs are also occasionally reported (van Zwieten *et al.* 1979, Hall *et al.* 1987, Li *et al.* 2013). In WT Sprague–Dawley rats, PCs begin to be detected at age 1–2 years, and the prevalence at 2 years is approximately 10% (Pace *et al.* 2002). The incidence is further increased by a variety of agents including high calorie diet, radiation, drugs and hormones (Tischler *et al.* 2004, 2014). In view of their innate proclivity to develop PCCs, we hypothesized that rats would *a priori* be superior to mice as a potential *Sdhb* tumor model. This communication describes the successful development of a new rat-derived xenograft and

cell culture model that closely mirrors the characteristics of *SDHB*-associated human PCPGs.

## Materials and methods

### Origin and validation of the model

Heterozygous *Sdhb*<sup>+/-</sup> Sprague–Dawley rats were generated by a commercial supplier (Cyagen Biosciences, Santa Clara, CA, USA) using the TALEN (transcription activator-like effector nuclease) technique (Merkert & Martin 2018). Four 'F0' founders were generated with various deletions in the rat *Sdhb* gene: a 1-base deletion in exon 1, a 13-base deletion in exon 1, a 7-base deletion in exon 2 and a 8-base deletion in exon 2. All of the mutations except the 1-base deletion successfully became germline on subsequent breeding. For each of the founder mutations, we tested liver tissue of heterozygous offspring for expression of rat *Sdhb* mRNA using a commercial TaqMan assay kit (Life Technologies). Enzymatic assays of liver tissue were also performed (Abcam Complex II Enzyme Activity Microplate Assay Kit). Finally, as a bioassay to confirm biological significance of the *Sdhb* deletions, we bred male and female *Sdhb*<sup>+/-</sup> heterozygotes to each other and examined gravid uteri as a test for homozygous embryonic lethality. Sperm from rats with all three germline deletions is cryopreserved at the Rat Resource and Research Center (RRRC) at the University of Missouri ([rrrc@missouri.edu](mailto:rrrc@missouri.edu)), where it will be publicly available.

### Development and harvesting of tumors

Thirty-five male *Sdhb*<sup>+/-</sup> rats with a 13-bp deletion in exon 1 (Supplementary Fig. 1, see section on [supplementary materials](#) given at the end of this article) formed the core of this study. Twenty-one of the animals were exposed to 5 Gy of gamma irradiation 1 week postnatally. The administration of postnatal irradiation was based on previous findings that irradiation of the parent animals contributed to the development of the rat-derived PC12 (Warren & Chute 1972) and mouse-derived MPC (Powers *et al.* 2000) PC cell lines. All were fed *ad libitum* on a standard rodent diet (Envigo/Harlan, Indianapolis, IN, USA) and were maintained until they were killed because of deteriorating health or were found dead. Necropsies were performed and the adrenal glands, pituitaries and carotid bodies were examined grossly and microscopically. Tissue from five PCs that appeared to be viable was injected subcutaneously into NSG mice as previously described (Powers *et al.* 2017). Xenografts of

the PC12 rat pheochromocytoma cell line (passage 40), (Greene & Tischler 1976) were similarly prepared to serve as controls in relevant analyses.

Primary tumors and xenografts in consecutive passages were examined histologically and immunohistochemically as previously reported (Powers *et al.* 2018). Antibodies utilized are shown in Supplementary Table 1. Immunoblots and electron microscopy were also performed as previously described (Powers *et al.* 2018).

### Cell cultures and development of cell lines

To generate primary cell cultures, minced xenograft tissue was dissociated in collagenase followed by trypsin (Powers *et al.* 2000). The dissociated cell suspension was plated in 35 mm culture dishes in a series of preliminary studies to test the effects of varied medium composition and O<sub>2</sub> concentration in attempting to establish cell lines. The utilization of xenografts to develop cell lines, rather than vice versa, served to expand tumor cell populations because the usually small primary tumors did not provide sufficient numbers of cells for adequate tests of growth conditions. It further provided xenografts comparable to human patient-derived xenograft (PDX) models, which are not derived from cell lines. This approach has been utilized by others for studies of human neuroblastomas (Persson *et al.* 2017).

Routine culture medium consisted of RPMI 1640 with 10% heat inactivated horse serum, 5% fetal bovine serum, glutamine and penicillin/streptomycin. This medium is employed in our laboratory to culture PC12 cells (Greene & Tischler 1976), normal rat chromaffin cells (Tischler *et al.* 1994) and mouse-derived MPC cells (Powers *et al.* 2000). Because SDH deficiency alters cells' nutritional requirements (Lussey-Lepoutre *et al.* 2015), we compared cell growth and survival in this medium vs an enriched medium supplemented with non-essential amino acids, fatty acids, uridine and pyruvate that we recently employed for primary cultures of a SDH-deficient gastrointestinal stromal tumor (GIST) (Powers *et al.* 2018). These basal and enriched media were compared to serum-free stem cell media consisting either of DMEM/F12 with B27 Supplement plus FGF (20 ng/mL) and EGF (20 ng/mL) or serum-free RPMI 1640 with the same B27 and growth factor supplementation. Also, based on the gastrointestinal stromal tumor study, which showed deleterious effects of O<sub>2</sub> on cell survival, we tested the effects of maintaining cultures in decreased oxygen concentrations (10%, 5% or 1%) compared to traditional 'normoxic' cultures (~20% O<sub>2</sub>, 95% air/5% CO<sub>2</sub>). In order to simultaneously compare

multiple O<sub>2</sub> concentrations, cultures were maintained in Billups-Rothenberg modular incubator chambers with pre-mixed gasses with increased N<sub>2</sub> to compensate for decreased O<sub>2</sub>. CO<sub>2</sub> concentration was constant at 5%. All cultures were maintained in a water-saturated atmosphere at 37°C. Double immunocytochemical staining for tyrosine hydroxylase (TH) and incorporation of bromodeoxyuridine (BrdU) (Tischler *et al.* 1992) was performed in order to distinguish the neoplastic chromaffin cells from fibroblasts, endothelial cells and other normal cell types. Two cell lines, designated RS0 (for rat *Sdhb* null) and RS1/2 (for *Sdhb* haploinsufficient), originated from cultures of xenografts derived from two different primary tumors and maintained in 5% O<sub>2</sub>.

### Whole genome sequencing

#### DNA extraction

Cell line DNA was extracted using a Qiagen Blood and Cell Culture DNA kit (catalogue number 13362) according to the manufacturer's instructions. Matched normal DNA was extracted from formalin-fixed, paraffin-embedded sections of kidneys from the individual rats in which the primary RS0 and RS1/2 tumors originated, using the Qiagen DNeasy Blood and Tissue kit (catalogue number: 69504) with a slightly modified protocol. Samples were deparaffinized in xylene and subjected to an additional ethanol wash to remove residual xylene. Proteinase K digestion was carried out at 56°C over 3 days instead of overnight, with 12 µL proteinase K added every 24 h. The optional RNase A treatment was also carried out using 4 µL of RNase (100 mg/mL) at the end of the 3-day incubation.

#### WGS library preparation and sequencing

Libraries were prepared at The University of Melbourne Centre for Cancer Research (UMCCR) using the Illumina® TruSeq™ DNA Nano library preparation method according to the manufacturer's instructions. Two hundred nanograms of DNA was used as input and a 550-bp insert size was targeted. Samples were sequenced in separate batches on the Illumina® Nova-Seq 6000. QC stats including the mean read count and insert size from each sample can be seen in Supplementary Table 2.

#### WGS alignment and quality control

BCL files were demultiplexed and converted to FASTQ files with Illumina® bcl2fastq (version 2.20.0.422) with predominantly default settings (including adapter trimming). The -no-lane-splitting flag was also added

as lanes were not used in this protocol. Alignment and variant calling steps were run as part of the validated bcbio-nextgen cancer somatic variant calling pipeline (version 1.1.3a) (<https://github.com/bcbio/bcbio-nextgen>). The bcbio-nextgen template that was used can be seen in Supplementary Table 7. The versions of all programs used by bcbio-nextgen are additionally shown in Supplementary Table 8. Briefly, the raw tumor and blood FASTQ files were first processed by Atropos (version 1.1.21) (Didion *et al.* 2017) to clip homopolymers (minimum 8 bases) from the ends of reads. Trimmed FASTQ files were aligned to the rat genome (version rn6) with BWA-mem (version 0.7.17) (Li 2013) with predominantly default settings. The two exceptions were that the -M flag was enabled to mark shorter split read hits as a secondary alignment and seeds with >250 occurrences were skipped (reduced from the default 500).

### WGS variant calling

Germline variants were called by Varscan (version 2.4.3) (Koboldt *et al.* 2012), GATK HaplotypeCaller (GATK version 4.1.2.0) (McKenna *et al.* 2010, DePristo *et al.* 2011) and Strelka2 (version 2.9.10) (Kim *et al.* 2018) callers. Somatic variants were called by the Varscan (version 2.4.3), Mutect2 (GATK version 4.1.2.0) (Cibulskis *et al.* 2013) and Strelka2 (version 2.9.10) variant callers. In both instances, a variant was accepted as true if it was detected by two of the three callers. Variant allele frequency was calculated from VCFs produced from bcftools call of samtools mpileup. All variants were inspected manually using the Integrative Genomics Viewer (IGV) (Robinson *et al.* 2011) and somatic variants with some germline presence in difficult-to-sequence regions of the genome were removed. The effect of somatic variants was annotated by ensembl VEP (version 95.3). Mutation signatures were generated using MutationalPatterns (Blokzijl *et al.* 2018). Signatures used were single base substitution (SBS) signatures from COSMIC v3 (Alexandrov *et al.* 2019, Tate *et al.* 2019).

### WGS copy number and structural variant calling

Somatic copy-number profiles were generated by running FACETS on the BCBio aligned BAM files with a rat-specific GC profile (calculated from the rn6 reference genome) and a cval of 1000. SVs were called separately with GRIDSS (version 2.0.0) (Cameron *et al.* 2017). The bam files used by GRIDSS were generated separately to those used for variant calling and CNV detection. Specifically, alignment was performed with BWA-mem (version 0.7.17) with default settings and duplicate marking was performed with

samtools (version 1.9). Structural variants were annotated with the StructuralVariantAnnotation R package (<https://github.com/PapenfussLab/StructuralVariantAnnotation>).

### Custom R analyses

All R analyses were performed with R (version 3.6.0) (<https://www.r-project.org/>). Circos plots were generated from GRIDSS and FACETS outputs using circlize (Gu *et al.* 2014).

### Comparison of syntenic regions between human and rat chromosomes

A table of human-rat gene homology (hg38 vs rn6) was downloaded from ensembl biomart (ensembl release 96) (Zerbino *et al.* 2018). The database was then filtered down to the rat chromosomes altered in the RS0 model (8, 5, 9 and 14p). Rat cytoband data (rn6) were downloaded from the UCSC annotation database (Raney *et al.* 2014). The proportion of rat-human syntenic genes on each chromosome arm was then calculated by dividing the number of high confidence syntenic genes between arms by the total number of genes on the corresponding human chromosome. GISTIC (version 2.0.23) (Mermel *et al.* 2011) was run on copy-number variation (CNV) profiles of *SDHB* tumors obtained from the TCGA and Castro-Vega papers (Castro-Vega *et al.* 2015, Fishbein *et al.* 2017). The proportion of rat-human syntenic genes was then compared with the frequency of chromosome arm loss (defined as >50% of a chromosome arm) as reported by GISTIC.

### Transcriptional profile

RNA sequencing was performed with an Illumina HiSeq 2000 at the Tufts genomics core facility. Paired-end RNA sequencing data were preprocessed using Trimmomatic (Bolger *et al.* 2014) to filter poor quality reads, then aligned using TopHat2 pipeline (Kim *et al.* 2013). FeatureCounts software (Liao *et al.* 2014) was used to map reads to genes, and edgeR (Robinson *et al.* 2010) was used to calculate RPKM (reads per kilobase of transcript per million mapped reads) (Powers *et al.* 2018).

### Consensus clustering analysis

Rat genes were first mapped to human genes using the biomaRt R package (Durinck *et al.* 2005). The rat RNAseq data were then normalized using the same procedure that

was applied to the human samples in the published TCGA analysis (Fishbein *et al.* 2017): rsem normalization, log<sub>2</sub> transform and then gene median centered. Genes with 0 reads across all rat samples were removed. The top 3000 most-variable genes by median absolute deviation were selected for cluster discovery using ConsensusClusterPlus as was done for the human clustering (Wilkerson & Hayes 2010, Fishbein *et al.* 2017). We then mapped 1699 rat genes to these 3000 human genes and used these 1699 genes to do a cross-species consensus clustering for 173 human samples and 3 rat samples.

### Metabolomics

Metabolomic analysis was performed as previously described (Powers *et al.* 2018). Briefly, unbiased metabolite profiling was performed using <sup>1</sup>H NMR, and <sup>13</sup>C-NMR was used to trace the metabolic fates of glucose and the contributions of glycolysis or anaplerotic TCA cycle pathways to the metabolite profile (Bruntz *et al.* 2017). Replicate s.c. xenograft nodules (each 1 cm in greatest dimension) were analyzed for RS0, RS1/2 and PC12. Pooled tissue from normal rat adrenal medullas was used as an additional SDH-intact control for <sup>1</sup>H NMR profiling.

### Statistics

Data are presented as mean ± s.e.m. with individual values displayed on graphs. Statistical analysis was carried out using GraphPad Prism software (GraphPad Software Inc). Significance was tested using unpaired Student's *t*-test, two tailed distribution with *P* < 0.05 set as significant.

### Study approval

All animal procedures performed in these studies were approved by the Institutional Animal Use and Care Committee of Tufts University and Tufts Medical Center.

### Genomics data availability

All WGS and RNA-seq data are available through NCBI short-read archive (SRA) (bioproject ID: PRJNA601534).

## Results

Liver tissue from heterozygous rats carrying each of the three germline *Sdhb* deletions showed approximately 50% reduced expression of *Sdhb* mRNA and enzyme

activity compared to age-matched WT rats and 68% of normal protein expression based on densitometry data. The biological significance of haploinsufficiency was confirmed by crossing *Sdhb*<sup>+/-</sup> X *Sdhb*<sup>+/-</sup> rats to generate homozygotes, which resulted in embryos developmentally stalled at ~5–6 days, as reported for *Sdhb*<sup>-/-</sup> mice (Piruat *et al.* 2004). Approximately 25% of 32 embryos were affected, consistent with the percentage of homozygotes predicted by Mendelian genetics (Fig. 1). In contrast, only one embryo of 31 was stalled in control specimens from WT rats. Because of the apparent functional equivalence of all three *Sdhb* deletions, we arbitrarily decided to focus on the largest (i.e. 13 base) deletion for colony expansion.

The mean lifespan of rats harboring the 13-base deletion was 88.5 ± 3.0 weeks (range 67–105, *n* = 15) for the non-irradiated vs 69 ± 4 weeks (range 38–104, *n* = 20) for the irradiated group (*P* = 0.0001) and the mean lifespan of 130 weeks for normal Sprague–Dawley rats according to the supplier, Taconic Laboratories (Rensselaer, NY, USA). Macroscopic PCs ~0.3–0.6 cm in greatest dimension were present in three irradiated rats and one non-irradiated. In addition, one irradiated rat developed a carotid body PG. Multiple microscopic adrenal medullary lesions that were cytologically identical to PCs but did not invade or compress the adrenal cortex were present in three irradiated and four non-irradiated animals. Although similar microscopic lesions would be classified as hyperplastic nodules in veterinary pathology literature (Tischler *et al.* 2014), they are classified here as micro PCs in light of current understanding based on molecular studies of small adrenal medullary nodules in humans (Korpershoek *et al.* 2014). Multiple pituitary adenomas were present in both groups of rats, as shown in Supplementary Table 3.

Two distinct, serially transplantable, PC xenograft models, which we have designated as RS0 and RS1/2, were derived at 84 weeks and 74 weeks, respectively, from macro PCs that arose in irradiated rats. RS0 xenografts histologically show sharply defined 'Zellballen' architecture, slightly clear cells and prominent blood vessels closely resembling human paragangliomas (Tischler & deKrijger 2015), while RS1/2 shows more diffuse growth (Fig. 2). As an initial screen for *Sdh* deficiency, both xenograft models and all primary tumors were stained immunohistochemically for SDHB protein (Dahia *et al.* 2005, van Nederveen *et al.* 2009). Only RS0 and the carotid body PG, which was too small to xenograft, were *Sdhb*-negative, as defined by loss of the granular cytoplasmic staining characteristic of intact SDHB (Figs 2C and 3B). Both were positive for SDHA,

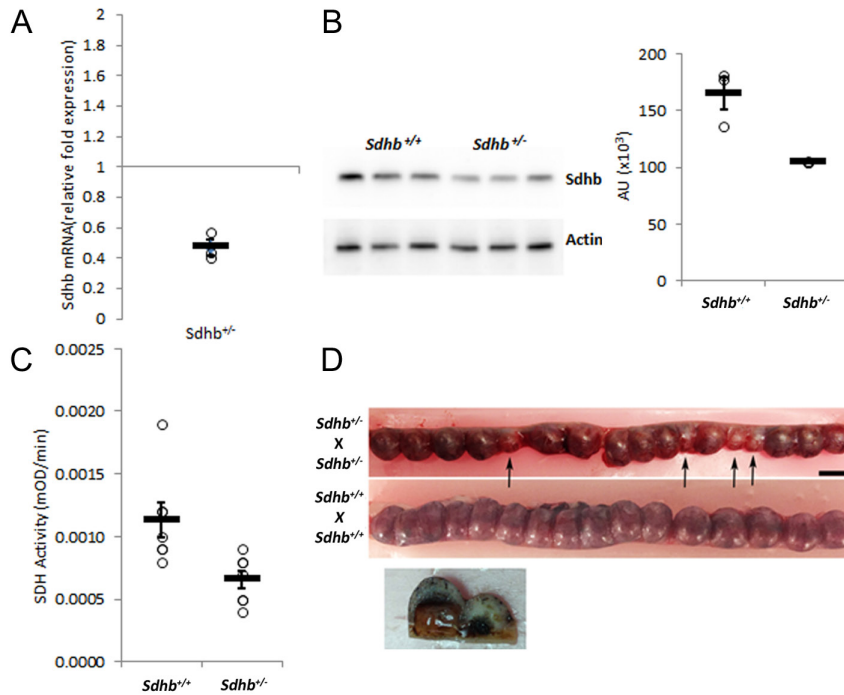
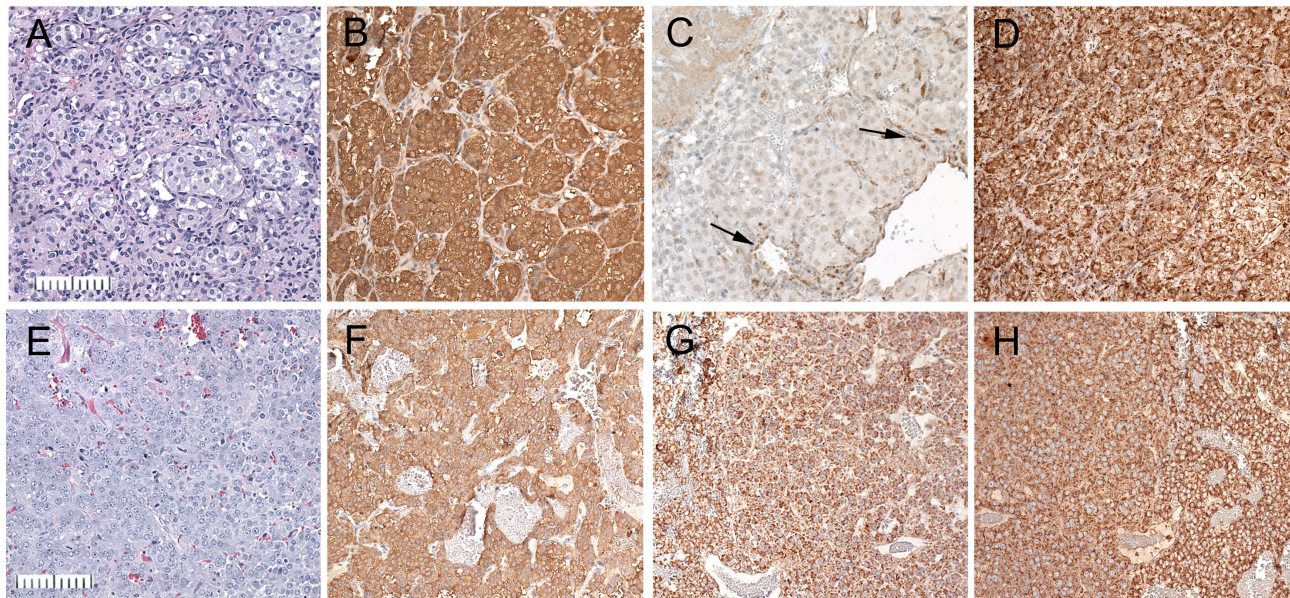


**Figure 1** Molecular and functional consequences of heterozygous *Sdhb* deletion. (A, B and C) Comparisons of liver tissue from 2-week-old heterozygous (*Sdhb*<sup>+/-</sup>) and WT (*Sdhb*<sup>+/+</sup>) rats. (A) Decreased *Sdhb* mRNA (*n* = 3 animals for each group, each point done in triplicate \**P* < 0.05). (B) Protein expression with densitometric analysis *n* = 3 \**P* < 0.05; and (C) decreased *Sdh* enzyme activity (*n* = 7 samples for each group, individual points done in duplicate) \**P* < 0.05. (D) Opened uteri from 12-day-old gravid rats showing stalled embryos in a representative heterozygous cross (top) compared to WT (bottom). Nine of 31 embryos examined were stalled in *Sdhb*<sup>+/-</sup> × *Sdhb*<sup>+/-</sup> vs 1 of 31 in WT pregnancies (*P* = 0.0125).

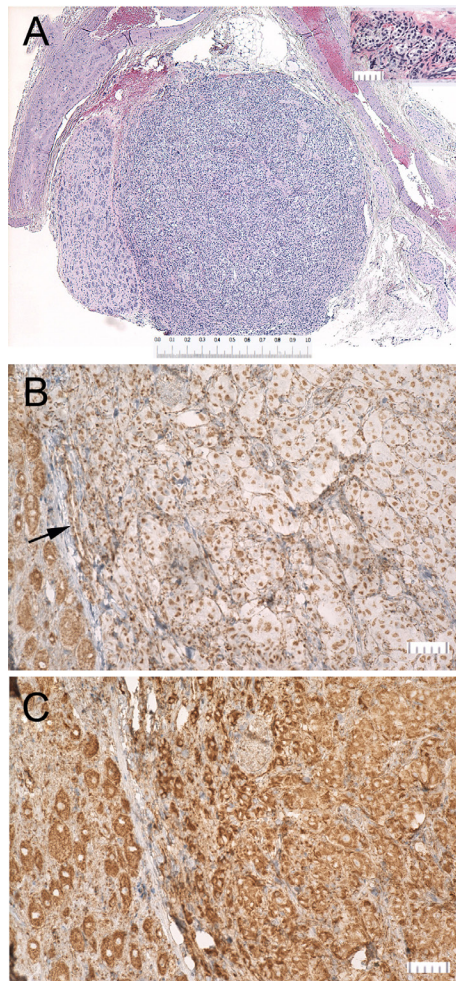
which is known to persist in SDH-deficient tumors caused by *SDHB* mutations (Korpershoek *et al.* 2011, Papathomas *et al.* 2015, Bezawork-Geleta *et al.* 2018). Additional immunohistochemical stains demonstrated diffuse immunoreactivity for tyrosine hydroxylase in

both RS0 and RS1/2. All pituitary adenomas showed intact staining for both SDHA and SDHB.

The most distinctive ultrastructural features of RS0 were relatively sparse secretory granules and cytoplasmic vacuoles similar to those in other SDH-deficient tumors



**Figure 2** Histology and immunohistochemistry of pheochromocytoma xenografts RS0 (A, B, C and D) and RS1/2 (E, F, G and H). (A and E) Hematoxylin and eosin stain (B and F). Tyrosine hydroxylase RS0 shows classic ‘zellballen’ pattern characteristic of pheochromocytomas and extra-adrenal paragangliomas, while RS1/2 shows diffuse growth. (C and G) SDHB. RS0 shows loss of granular cytoplasmic staining for *Sdhb* in tumor cells and retained dark granular staining in endothelial cells (arrows). In contrast RS1/2 shows positive staining in both tumor and endothelial cells. (D and H) SDHA. Both RS0 and RS1/2 show positive staining in tumor cells and endothelium. Bar = 100 µm.

**Figure 3**

Carotid body paraganglioma. (A) Carotid bifurcation containing a paraganglioma (center) and adjacent superior cervical ganglion (left); Bar = 1 mm. Inset shows the entire normal carotid body from an 18-month-old *Sdhb*<sup>-/-</sup> rat (Bar = 50  $\mu$ m). (B) Immunohistochemical stain for SDHB showing loss of granular cytoplasmic staining in tumor cells and retained dark granular staining in endothelial cells (arrow) and SCG neurons. (C) Tumor cells, neurons and endothelial cells show granular staining for SDHA.

(Powers *et al.* 2018). RS1/2 showed larger and more numerous secretory granules than RS0 and no cytoplasmic vacuoles (Fig. 4). An additional difference was that the mitochondria in some RS0 cells showed prominent tubular or branched cristae and were sometimes also elongated (Fig. 4 inset). These reactive changes have been observed in some SDH-deficient human tumors (Szarek *et al.* 2015) and can result from altered redox balance (Cogliati *et al.* 2016). However, the marked mitochondrial swelling and degeneration reported in the human tumor specimens and some other models (Douwes Dekker *et al.* 2003, Szarek *et al.* 2015, D'Antongiovanni *et al.* 2017, Powers *et al.* 2018) were not seen. The relatively mild

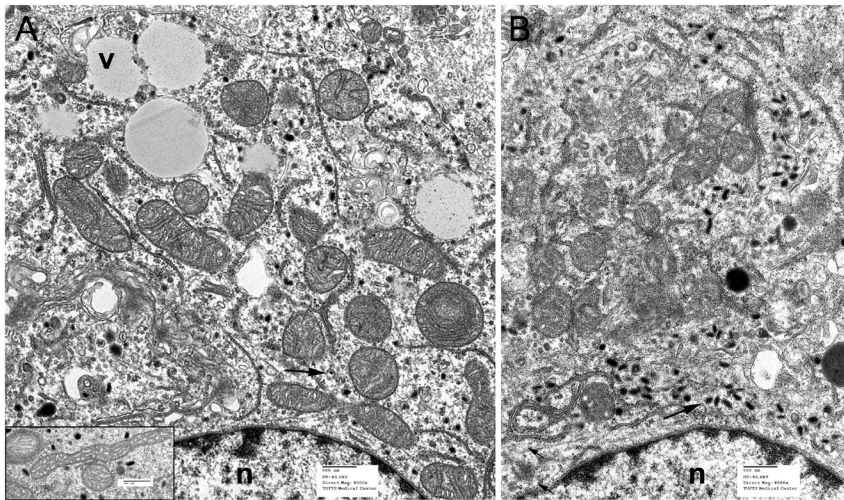
mitochondrial changes in RS0 cells are consistent with a recent study indicating that immortalized *Sdh*-null cells derived from rodent chromaffin cells may be less bioenergetically compromised than *Sdh*-compromised cells of other types (Kluckova *et al.* 2020).

### Cell culture and establishment of cell lines

Preliminary studies showed that cells derived from neither xenograft model would produce a cell line in an atmosphere of 95% air/5% CO<sub>2</sub> and routine RPMI culture medium with 10% horse serum/5% fetal bovine serum. Under those conditions, RS0 cells rapidly accumulated large cytoplasmic vacuoles and died over a period of approximately 2 weeks. In contrast, RS1/2 cells survived for months and did not form vacuoles but slowly dwindled. Optimal cell survival was obtained in 5% O<sub>2</sub>, consistent with the beneficial effect of low O<sub>2</sub> previously observed with SDH-deficient GIST (Powers *et al.* 2018). However, this was still insufficient to develop cell lines. We, therefore, next tested combinations of 5% O<sub>2</sub> together with lowered-to-absent serum in medium with stem cell-promoting supplements (Persson *et al.* 2017). Under those conditions, RS0 cells proliferate as a continuous cell line in uncoated plastic culture dishes in serum-free medium as free-floating spheres with a doubling time of approximately 14 days (Fig. 5). A similar-appearing cell line growing in 5% O<sub>2</sub> was also derived from RS1/2 cells. However, the RS1/2 line requires serum in a low concentration (1% HS/0.5% FBS). For both cell types, preliminary studies showed the use of RPMI 1640, as the base medium is slightly preferable or equivalent to the DMEM/F12 mixture widely used in stem cell cultures.

### Whole genome sequencing

We performed WGS to verify genetic loss of WT *Sdhb* and to identify additional somatic changes in RS0 and RS1/2 tumor cells. WGS was initially performed on RS0 xenograft tissue; however, some ambiguities resulted from the presence of mouse DNA sequences introduced by the host animal. In order to obtain cleaner data, WGS was repeated using DNA extracted from RS0 and RS1/2 cultured cell lines devoid of mouse stromal and immune cells. Focused analysis of sequence coverage of *Sdhb* identified the expected 13-bp deletion in exon 1 plus a 729-bp deletion immediately upstream of the *Sdhb* promoter in the RS0 germline DNA (Fig. 6A). As shown in Fig. 6A, there is clear evidence of a 729-bp hemizygous deletion in both the normal germline DNA and tumour DNA of RS0 and

**Figure 4**

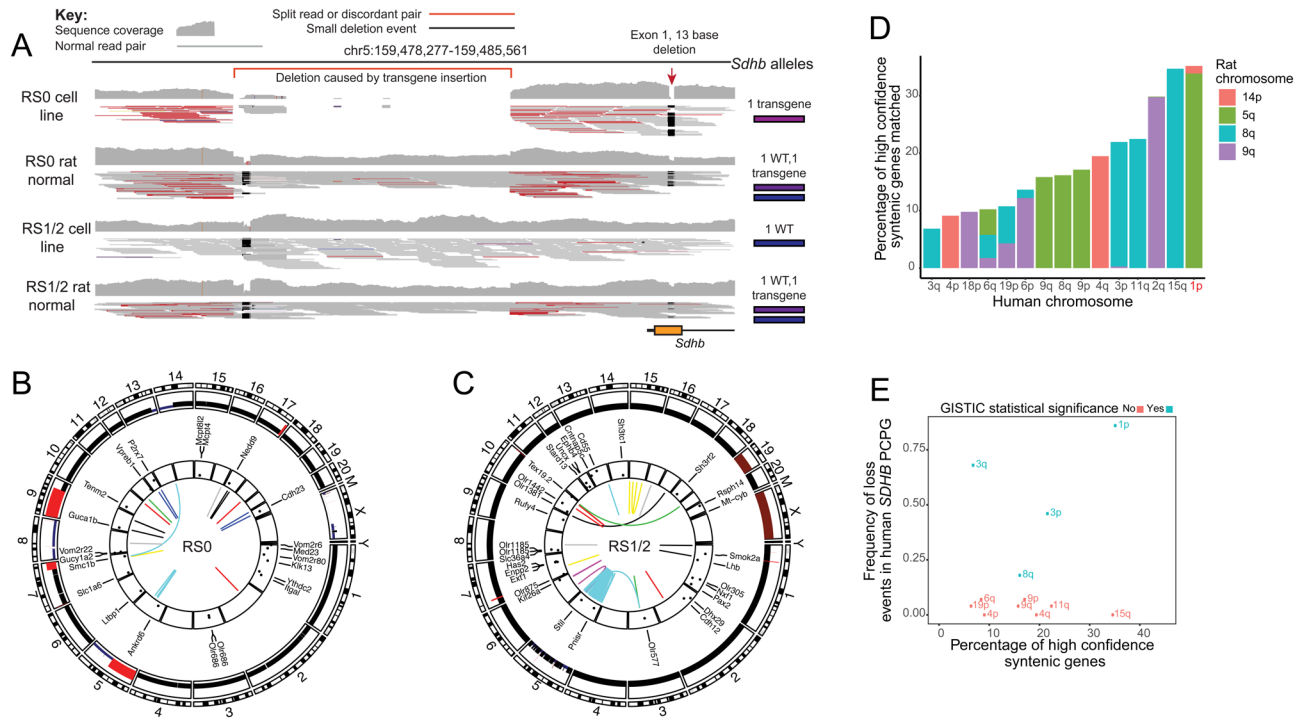
Electron micrographs of RS0 (A) and RS1/2 xenografts (B). Arrows indicate neuroendocrine secretory granules; v, cytoplasmic vacuoles; n, nuclei. Characteristic features of RS0 are cytoplasmic vacuoles and sparse, often tiny secretory granules. In contrast, RS1/2, which is not SDH-deficient, has larger secretory granules and lacks cytoplasmic vacuoles. Inset at left shows elongated mitochondria with tubular cristae that were seen in some RS0 cells.

RS1/2. The deletion is inferred by the sharp reduction in read depth at the genome co-ordinates upstream of *SDHB* as indicated and the paired reads that span the deletion, which are marked in red. The deletion was certainly a result of the TALEN process and not radiation. Inference of read coverage, and genome-wide copy-number analysis for cell line RS0 showed somatic segmental loss of chr5 including the WT *Sdhb* allele (Fig. 6B). In cell line RS1/2, we observed a chromothripsis involving chr5 resulting in loss of the TALEN-edited non-functional *Sdhb* allele but retention of the *Sdhb* WT allele (Fig. 6C). These data are in keeping with the negative SDHB protein expression in RS0 but positive SDHB staining in RS1/2.

**Figure 5**

Cell cultures of RS0 cells grown in serum free medium. (A) Darkfield photomicrograph showing typical appearance of tumor cell spheroids, which often form on top of cells attached to the culture dish, then detach and grow suspended in the medium. (B) Cytocentrifuge preparation showing a representative microspher immunohistochemically stained for tyrosine hydroxylase (red cytoplasm) and bromodeoxyuridine (BrdU, black nuclei) after 7 days of BrdU labeling. White circles within the microspher are unlabeled nuclei. Arrow indicates a labeled mitotic figure, indicating that incorporating BrdU can go on to divide. Bar = 100 µm.

Both RS0 and RS1/2 cell lines had low mutation burden (RS0, 0.8 mutations/Mb; RS1/2 0.96 mutations/Mb). The highest proportion of base substitutions involved C>T transitions, but no dominant mutational signatures were observed in either cell line (Supplementary Fig. 2). With respect to mutations and structural alterations, no somatic lesions in gene orthologues previously found to be mutated in human PCPG were identified (Supplementary Tables 4 and 5). A ~108-kb homozygous deletion involving exon 1 of *Cdkna* and complete loss of *Cdkn2b* was identified in cell line RS0. Inspection of the WGS sequence data in the matched xenograft, however, showed no evidence of this deletion event in the original RS0 tumor, therefore it was unlikely to be a founding event in RS0 tumor cells (Supplementary Fig. 3). In RS1/2, two mutations of unknown significance were detected in known cancer genes (*Stil* and *Ext1*). Furthermore, numerous structural alterations were identified in cell line RS1/2 involving chromothripsis of chromosome 5. Breakpoints were detected within cancer genes *Arid1a*, *Nfib* and *Psip1*, the latter involving a gene fusion with *Zbtb48*. The principal driver gene mutation in RS1/2 is not apparent but may involve haploinsufficiency of one or more of these cancer genes or other genes on chr5. Interestingly, in cell line RS1/2 we observed a missense mutation at 10% variant allele frequency in cytochrome B (Mt-cyb). Despite the paucity of pathogenic mutations in both cell lines, we observed large segmental copy-number loss events in RS0 that are syntenic with frequently altered chromosomal regions in human *SDHB*-associated PCPG tumors (Fig. 6D and E). These events included syntenic loss of human chr1p, chr2q, chr3, chr8q and chr18p. We reasoned that these structural events are likely to be important in co-operating with *SDHB* loss of function

**Figure 6**

WGS of RS0 and RS1/2 tumor cell lines and their matched germline DNA. (A) Genome viewer snapshot of sequence coverage spanning exon 1 of *Sdhb* and the genomic region immediately 5' of *Sdhb* (~1.4 kb in total). A 13-bp deletion within exon 1 of *Sdhb* was detected in the germline DNA of both RS0 and RS1/2. The exon 1 deletion was present in all sequencing reads in tumor cell line RS0, indicating that the WT *Sdhb* allele had been lost during tumorigenesis. Conversely, the TALEN-edited *Sdhb* allele was lost during tumorigenesis of tumour cell line RS1/2. In addition to the exon 1 deletion, a larger 729-bp deletion was also detected upstream of *Sdhb*, indicated by the presence of discordant or split reads spanning the deletion breakpoint (these reads are highlighted in red). The deletion upstream of *Sdhb* is also supported by a precipitous drop in sequence coverage spanning the 729-bp deletion. Like the 13-bp exon 1 deletion, the 729-bp deletion was detectable in the germline DNA of RS0 and RS1/2, indicating that it was introduced by TALEN gene-editing. (B) A circos plot describing the somatic alterations that occurred in the formation of RS0. From outside to inside, tracks are as follows: rat cytoband, total copy-number variation (CNV) as called by FACETS (black signifies  $n = 2$ , red signifies  $n > 2$  and blue signifies  $n < 2$ ), names of genes called by BCBio ensemble variant calling as having a coding mutation, the allele frequency of these mutations and the innermost track represents the structural variants called by GRIDSS. (C) A circos plot describing the somatic alterations that occurred in the formation of RS1/2. Tracks are in the same order as described in (B). (D) The percentage of high confidence orthologous genes matched between rat and human comparing chromosome arms called by FACETS as being altered in RS0 (either gain or loss). (E) Comparison of high confidence orthologous genes from D (further filtered only to chromosomal loss events in RS0) against the frequency of chromosomal arm level loss events in human *SDHB* PCPG as determined by GISTIC. Human copy-number variation (CNV) data were taken from publicly available copy-number profiles cited in the Materials and methods section. Chromosome arms colored in blue were called as statistically significantly altered by GISTIC (false discovery rate <0.05). Chromosome arm level losses of 1p, 3q, 3p and 8q are frequent and statistically significant events in human PCPG. These regions are overlapping with syntenic genomic regions that have undergone somatic loss in rat model RS0.

to promote tumorigenesis, and provide further evidence that RS0 has the genomic hallmarks of human *SDHB* pheochromocytoma.

### Metabolite profile

The presence of SDH deficiency was confirmed by high levels of succinate accumulation (Table 1). In RS0 xenografts, succinate was the third most abundant metabolite, in contrast to both RS1/2 and adrenal medulla. Lactate was the most abundant metabolite measured, consistent with increased production of lactate

and induction of lactate dehydrogenase in SDH-deficient tumors and cell lines (Lussey-Lepoutre *et al.* 2015). *In vivo*  $^{13}\text{C}$ -glucose labeling showed robust incorporation of glucose into lactate and succinate and lesser incorporation into alanine and glutamate. The labeled glutamate contained almost the same amounts of ( $^{13}\text{C}$ 2-4,5)Glu and ( $^{13}\text{C}$ 2-2,3)Glu isoptomers, indicating approximately equal activity of pyruvate dehydrogenase (PDH) and pyruvate carboxylase (PC), respectively (Lussey-Lepoutre *et al.* 2015, Bruntz *et al.* 2017). This result is consistent with previous studies showing increased utilization of the anaplerotic pathway catalyzed by PC in *Sdh*-deficient mouse cell lines (Lussey-Lepoutre *et al.* 2015).

**Table 1** NMR metabolomic profiles of RSO, RS1/2 xenografts and rat adrenal medulla (RAM).

	RAM (20 pooled)		RSO (n = 4)		RS1/2 (n = 3)	
	Mean ± S.E.M.		Mean ± S.E.M.		Mean ± S.E.M.	
The ten most abundant detectable metabolites (μmol/mg of tissue)						
Epinephrine	16.15					
Norepinephrine	12.33		15.18 ± 3.66		Norepinephrine	33.87 ± 29.41
Glucose	2.31		12.11 ± 2.69		Lactate	11.45 ± 2.18
Lactate	0.89		5.99 ± 1.19		Taurine	10.38 ± 0.83
Taurine	0.61		3.47 ± 0.75		Ascorbate	7.611 ± .42
ATP (or ADP)	0.59		2.57 ± 0.58		myo-Inositol	6.33 ± 2.80
Ascorbate	0.44		2.57 ± 0.64		Glutamate	4.16 ± 0.97
AMP	0.30		2.08 ± 0.45		Dopamine	2.55 ± 2.04
ADP (or ATP)	0.21		1.39 ± 0.28		O-Phosphoethanolamine	2.06 ± 0.25
Glutamate	0.17		1.29 ± 0.34		AMP	1.85 ± 1.39
<b>Succinate</b>	0.01		1.21 ± 0.26		Betaine	1.83 ± 0.31
30 of 67					<b>Succinate</b>	0.29 ± 0.10
Catecholamine and metabolite profile (μmol per mg of tissue)					30 of 67	
Dopamine	0.07					
3,4-Dihydroxybenzeneacetate <sup>a</sup>	0.00		0.38 ± 0.08			2.55 ± 2.04
Norepinephrine	12.33		0.05 ± 0.02			0.23 ± 0.05
Normetanephrine	0.00		0.06 ± 0.03			33.87 ± 29.41
Epinephrine	16.15		0.02 ± 0.01			0.00 ± 0.00
Tyrosine	0.00		0.00 ± 0.00			0.81 ± 0.78
			0.11 ± 0.01			0.03 ± 0.00

<sup>a</sup>3,4-Dihydroxyphenylacetic acid (DOPAC).

Similar to SDH-deficient human paragangliomas, the catecholamine profile of RSO xenografts showed a predominance of dopamine, low levels of norepinephrine and undetectable epinephrine (Table 1).

### Transcriptome and immunoblots

RSO xenografts show high expression of canonical cluster 1 markers associated with the Hif2a regulatory network (Table 2) and with hereditary *SDHB* mutations in the Cancer Genome Atlas (TCGA) (Fishbein *et al.* 2017) and previous comparable studies (Burnichon *et al.* 2011, Castro-Vega *et al.* 2015). These include Hif2a (also known as *Epas1*) and its targets including *Vegfa* and *Adm* (Table 2, and complete list in Supplementary Table 6). RNAseq also confirms the near total loss of *Sdhb* mRNA in RSO xenografts, with residual low level expression consistent with the presence of blood vessels and other non-neoplastic cells (Fig. 2C). A novel finding is the presence of concomitant, though lesser, reduction in mRNA transcripts of other SDH subunits (Supplementary Table 6). Surprisingly, RS1/2 also shows modest reductions in multiple SDH subunits despite the presence of immunoreactive SDHB and a relatively low level of Hif2a (Supplementary Table 6).

To further test how expression of the critical markers HIF2A and SDHB at the protein level correlates with immunohistochemical and RNAseq data, immunoblots of RSO and RS1/2 xenografts were probed for these proteins in parallel with their corresponding cell lines. The PC12 rat pheochromocytoma, which is known to express HIF2A (Bechmann *et al.* 2019) but be *Sdhb*-intact, served as a positive control. In xenograft tissue, RSO shows high HIF2A expression consistent with its high expression at the RNA level, while expression in RS1/2 is relatively low. Interestingly, in cell cultures this pattern is reversed as a result of increased expression in RS1/2. Cell cultures

also show that protein expression is not completely unresponsive to O<sub>2</sub> concentration in either RSO or RS1/2 cells. Importantly, however, expression in RSO cells at 5% O<sub>2</sub>, which approximates the concentration in solid tumors (Carreau *et al.* 2011), is comparable to expression in xenograft tumor tissue (Fig. 7). Immunoblots confirm the loss of SDHB in RSO cells, while SDHA is both retained and slightly increased in primary *Sdhb*<sup>-/-</sup> vs *Sdhb*<sup>+/-</sup> xenografts (Fig. 7A) and in RSO compared to RS1/2 cells (Fig. 7B). This increase may be related to a reported role of *Sdha* in an alternate assembly of respiratory complex 2 that decreases metabolite synthesis and cell proliferation in response to knockdown of SDHB (Bezawork-Geleta *et al.* 2018).

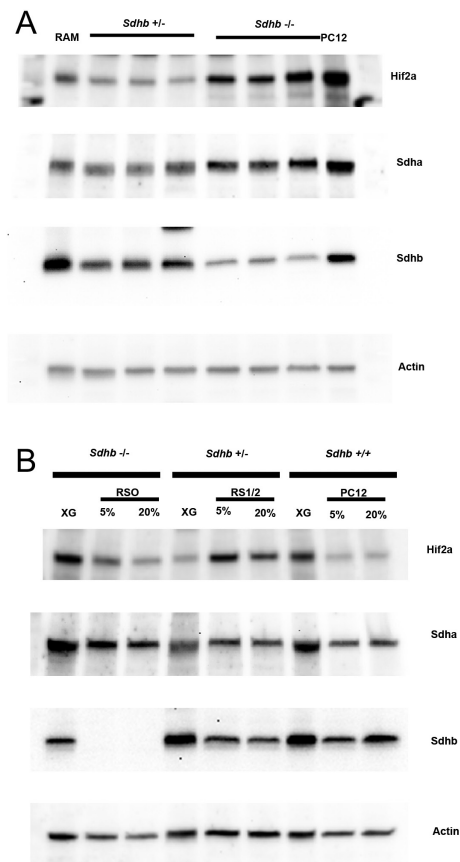
### Cross-species clustering analysis

In the TCGA study, consensus clustering divided 173 human samples of PC/PGs tumors into four molecularly defined groups: a kinase signaling subtype, a pseudohypoxia subtype, a *WNT*-altered subtype and a cortical admixture subtype (Fishbein *et al.* 2017). We performed cross-species consensus clustering analysis to test where among those subtypes the rat tumor samples would correspond. To do this, the rat RNAseq data were first analyzed to identify human homologs among the 3000 most highly expressed SDHB-associated genes used in the TCGA study. This yielded a set of 1699 overlapping genes. Consensus clustering was performed as described in Methods. First, using the 1699 gene sample set to re-analyze the TCGA data, the vast majority of the human TCGA data sets clustered to the same group as originally described for the 3000 genes in the published TCGA study, indicating that the reduced consensus sample set does not adversely affect the clustering results. When all three rat samples were then clustered with the human samples, the rat samples were all clustered together, indicating that the rat samples are more similar to each other than to

**Table 2** RNAseq data comparing expression of *Epas1* and genes in its regulatory network in RSO and RS1/2 xenografts and pooled rat adrenal medullas (RAM).

Gene <sup>a</sup>	RAM (RPKM <sup>b</sup> )	RSO (RPKM)	RS1/2 (RPKM)	RSO/RAM	RS1/2/RAM
<b>Epas1</b>	80.01	<b>1074.63</b>	76.62	<b>13.43</b>	0.96
<i>Egln3</i>	1.44	23.29	0	16.17	0
<i>Bhlhe40</i>	10.99	114.0	11.77	10.37	1.07
<b>Vegfa</b>	51.43	<b>607.36</b>	62.04	<b>11.81</b>	1.21
<i>Twist1</i>	1.86	14.82	0.50	7.95	0.27
<i>Serpine1</i>	2.65	241.62	5.9	91.18	2.23
<i>Adora2a</i>	5.41	593.88	2.99	109.78	0.55

<sup>a</sup>Genes listed are from the NCBI HIF-2-alpha transcription Network (Biosystems NCBI, <https://www.ncbi.nlm.nih.gov/biosystems/137956?Sel=geneid:2034#show=genes>). Those with the highest in the ratios in RSO to RAM are shown. <sup>b</sup>Raw data are expressed as reads per kilobase of transcript per million mapped reads (RPKM). The constitutive expression of *Epas1* in RAM is consistent with findings in normal embryos (Favier *et al.* 1999).

**Figure 7**

Immunoblots for HIF2A, SDHB and SDHA. (A) Representative immunoblot comparing levels of HIF2A, SDHB and SDHA in RSO and RS1/2 xenografts. A single immunoblot from a 4–15% gradient polyacrylamide gel was consecutively probed, stripped and re-probed for each of the indicated proteins. RAM (rat adrenal medulla) and PC12 (xenograft produced in NSG mouse from passage 40 cells) were run as controls. (B) Representative immunoblot comparing RSO, RS1/2 and PC12 xenograft tissue (XG) to corresponding cell lines in culture maintained in either 5% or 20% O<sub>2</sub>. Single immunoblot stripped and re-probed as in panel A.

the human samples (Supplementary Fig. 4A). To avoid this complication, each rat sample was clustered individually with the human samples in order to minimize the species effects. When this was done, all three rat tissue samples, rat adrenal medulla, RSO and RS1/2, were clustered with the human pseudohypoxic cluster (Supplementary Fig. 4B, C and D).

## Discussion

We have developed two serially transplantable xenograft and cell line PC models, which we call RSO and RS1/2, from rats with a heterozygous germline deletion in *Sdhb*. RSO, which is *Sdh* deficient, is genomically comparable to its human counterpart and differs from existing models in

that it arose in an animal with a hereditary *Sdhb* mutation. RS 1/2, which was derived from a different primary PC, has lost the mutated *Sdhb* allele retains one WT allele. RS1/2 shows some succinate accumulation consistent with haploinsufficiency but is not fully *Sdh* deficient. It differs from RSO in showing intact staining for SDHB, a greater degree of neuroendocrine differentiation and a largely different transcriptome, although some markers are shared. RS1/2 serves both as a control for studies of RSO and as a potential tool for studying patients' tumors that may be haploinsufficient for SDH but have undetermined driver mutations. The main focus of this communication is on RSO and RS1/2 xenografts, which would have the greatest immediate relevance to human tumors *in vivo*. Subsequent publications will entail detailed characterization of the cell lines and their applications.

RSO and RS1/2 originated and have been maintained in the form of xenografts that were never in cell culture – that is, the equivalent of early passage human PDX models. They may therefore be especially valuable for pre-clinical drug testing. These xenografts grow slowly enough to faithfully represent aggressive human PGs, but rapidly enough to be practical for testing and imaging. Since there is a pending clinical trial of an EPAS1 inhibitor for metastatic PG (NCT02974738) (Tella *et al.* 2017), RSO xenografts might be immediately relevant for pre-clinical drug testing as well as basic research. Features that RSO xenografts share with SDH-deficient human PGs include identical histology (Tischler & deKrijger 2015), loss of SDHB protein with retention of SDHA (Korpershoek *et al.* 2011, Papatthomas *et al.* 2015) and expression of the neuroendocrine markers TH and chromogranin A (Letouze *et al.* 2013). The presence of these markers indicates that they are not an irrelevant or dedifferentiated cell type, while the relatively low expression is comparable to that in human tumors (Letouze *et al.* 2013). Shared molecular markers include accumulation of a high concentration of succinate, metabolic rewiring and a transcriptional profile including high expression of multiple markers directly sensitive to impaired electron transport or hypoxia. The latter include Hif2a and its downstream targets including Vegfa.

Several highly expressed genes in RSO xenografts are strong direct indicators of adaptive responses to the pathobiology of SDH deficiency. These include *Cox4i2* (cytochrome c oxidase subunit 4i2), which catalyzes electron transfer from reduced cytochrome c to oxygen, and *Ndufa4l2* (mitochondrial complex associated like 2), which encodes a subunit of Complex I of the respiratory chain. These markers are two of the three 'exemplar genes'

cited in the TCGA study for being consistently associated with pseudohypoxia in human PGs (Fishbein *et al.* 2017) and *Ndufa4/2* is of particular interest in that complex 1 activity is reportedly upregulated in *SDHB* mutated human PGs (Pang *et al.* 2018). However, the third exemplar gene, *Ntn2* (netrin-G2) which modulates development of neuronal circuits and is less obviously related to SDH deficiency, is also not highly expressed in RS0. This is the case for many, but not all, other apparent mismatches. Notably, the hypoxia-inducible factor *Egln3* (egl-9 family hypoxia-inducible factor 3, also known as Phd3), which is highly expressed in RS0, has been strongly associated with pseudohypoxia in *VHL* but not *SDHB*-mutated human tumors (Burnichon *et al.* 2011). While the transcriptome of RS0 is not a perfect match to human cluster 1, many of the mismatches that are peripherally related to the primary functional defects might reflect different species, different anatomic sites (Fliedner *et al.* 2018) and different cells of origin within an anatomic site or different developmental stages in which the human vs rat tumors originate. A particular finding suggesting an influence of developmental stage is the overexpression of *Ret* in RS0. *Ret* is widely expressed in early adrenal development but is then downregulated in maturing chromaffin cells and maintained in neurons (Powers *et al.* 2009).

An important aspect of this study is the use of normal adrenal medullary tissue as a reference. This contrasts with profiling studies of human PCPG, in which the different tumor clusters were compared only to each other and to an unrelated reference DNA (Burnichon *et al.* 2011, Fishbein *et al.* 2017). By specifically focusing on large differences between a tumor and its tissue of origin, rather than solely between subsets of tumors, it may be possible to find new drug targets in the HIF2A transcription network that entail fewer systemic side effects than targeting HIF2A itself. Hypothetically, those systemic effects could include depletion of normal stem cells (Hammarlund *et al.* 2018). A disadvantage of normal adrenal medulla is the potential confounding effect of residual adrenal cortex, which is inevitably present, in some analyses. However, by selectively focusing on large differences in specific markers, it is possible to discern distinctive characteristics of the cells of interest, as shown in the TCGA 'cortical admixture' cluster. In addition, it may be possible to calculate the proportion of cortical contamination (Fliedner *et al.* 2010). An interesting observation in this study was that carefully dissected normal rat adrenal medulla clustered in the pseudohypoxic group. While this might partly represent an artifact of cross-species clustering, it is consistent with previous reports of HIF2A

expression in normal sympathoadrenal development and function (Favier *et al.* 1999, Richter *et al.* 2013).

Although PDX-like xenografts are an excellent model for pre-clinical drug testing (Shultz *et al.* 2014), cell lines are needed for mechanistic studies. Availability of cell lines also makes models accessible to many more researchers than those who would work with xenografts alone. Our cell culture studies were undertaken both to establish cell lines from RS0 and RS1/2 xenografts and to test whether non-conventional culture conditions that we previously demonstrated to be favorable to survival of cells from a unique SDH-deficient human GIST (Powers *et al.* 2018) would apply to these new models. Our results replicated our previous finding that routine 'normoxic' culture conditions are deleterious. In addition, we demonstrated an adverse effect of serum, which has been reported by others in PDX-derived cultures of human neuroblastoma. The deleterious effect of oxygen is not surprising because  $pO_2$  *in vivo* has been measured at ~41 mm Hg in normal liver (equivalent to ~5%  $O_2$ ) and ranged from 0–54 mm Hg in tumors of different types (Carreau *et al.* 2011). In both normal and neoplastic cells, low  $O_2$  may help to maintain stem cells (Hammarlund *et al.* 2018). The beneficial effects that we observed with low or absent serum and stem cell-promoting medium supplements in establishing the RS0 and RS1/2 cell lines is entirely consistent with a recent report by Persson *et al.* that neuroblastoma cells cultured from human patient-derived xenografts differentiate in serum but remain tumorigenic when propagated in stem cell medium (Persson *et al.* 2017). It remains to be determined how these new insights will affect future efforts to develop cell lines of human PC and PG. However, our cell culture findings and those of others suggest a need for radical departure from conventional methods, perhaps especially for SDH-deficient tumors. This applies both to model development and pre-clinical drug testing, which is usually conducted in 95% air/5%  $CO_2$  and may thereby exaggerate the efficacy of many chemotherapeutic agents (Carreau *et al.* 2011). However, individual tumors and different tumor types (Burgess *et al.* 2017) will likely require individualized culture conditions. It is well known that genetic and epigenetic characteristics of individual cancers and types of cancer can dictate different approaches to treatment (Burgess *et al.* 2017).

Multiple factors likely contributed to the development of these new rat models, including the innate proclivity of aging rats to develop PCs, combined with postnatal irradiation. Both of these have previously been reported for other rodent PC models (Powers *et al.* 2000). Very little is known about the genetic changes underlying the general

susceptibility of rats to pheochromocytomas. The most extensively characterized and relevant model is MENX, which is caused by a loss-of-function mutation in *Cdkn1b*, which encodes the cyclin-dependent kinase inhibitor p27Kip1. This change was not found in RS0 or RS1/2, and, to our knowledge, whole genome sequencing has not been performed on MENX rats. Comparisons of these might yield useful information. It is plausible that, in our models, radiation caused somatic genetic changes that accelerated the growth of spontaneous PCs and caused one of the tumors to become SDH deficient. However, consistent with human PCPG, both RS0 and RS1/2 had very low mutation burdens, very few gene coding mutations and relatively stable genomes. Chromothripsis of chr5 caused by a single catastrophic event was likely important for tumorigenesis of RS1/2, and exposure to ionizing radiation may be implicated. However, chromothripsis is also a feature of some primary human PCPG (Flynn *et al.* 2015), which ostensibly arises in the absence of radiation exposure.

As in human PCPG, few co-operative DNA mutations could be found in rat PC and the tumor genome is typified by recurrent chromosomal arm level loss events resulting in presumed haploinsufficiency of multiple genes. Chromosomal loss events syntenic with recurrently altered chromosomal regions in human SDHB-associated PCPG indicate that the RS0 model faithfully represents the genome of human PCPG and therefore may be useful for dissecting therapeutic vulnerabilities based on common co-operative somatic changes. A homozygous deletion was detected in cell line RS0 involving two neighboring tumor suppressor genes *Cdkn2a* and *Cdkn2b*. This event is predicted to cause complete loss of function of the protein p19ARF, which is encoded by an alternative reading frame of *Cdkn2a*. p19ARF is a negative regulator of MDM2 and loss of p19ARF is known to cause indirect suppression of p53 through the ARF-MDM2-p53 tumor-suppressor axis (Eischen *et al.* 1999). However, because the *Cdkn2a* deletion was not detected in the RS0 xenograft, it most likely was not involved in early tumorigenesis of RS0. The existence of the *Cdkn2a* deletion may further increase the relevance of the RS0 cell line as a pre-clinical model because *p16INK4A/Cdkn2a* gene expression is frequently downregulated in human PCPG, either by genetic abnormalities or promoter methylation (Muscarella *et al.* 2008), and is associated with poor prognosis (Kiss *et al.* 2008).

Two hypotheses were implicit in the protocol design and outcome this study. The first is that unpredictable haploinsufficiencies resulting from radiation damage or other causes may account for features required for

tumorigenesis in addition to loss of *Sdhb*, likening the RS0 model to human PCPG. This might explain why previous ('clean') gene knockouts of SDH subunits in various combinations with targeted loss of selected tumor suppressors, for example, in mice, have failed, because of their inability to achieve these other genetic effects. The second hypothesis is that rats are innately more susceptible than mice to this type of tumor. It is therefore of interest that we unsuccessfully tested a similar protocol in mice prior to undertaking the rat project. The radiation protocol was used initially by Jacks *et al.* to increase the frequency of pheochromocytomas in heterozygous Nf1 knockout mice (Jacks *et al.* 1994) and then in our laboratory to establish the derivative MPC cell lines (Tischler *et al.* 1995, Powers *et al.* 2000). Even more important than radiation, outbreeding of the 129SV<sup>Nf1+/-</sup> mutation carriers to WT C57BL6 mice was essential for tumorigenesis, possibly reflecting different levels of tumor suppressor genes expressed in different mouse strains (Hawes *et al.* 2007). In attempting to develop a *Sdhb*-null mouse model, we followed exactly the protocol previously used to develop MPC cells. We obtained four male 129SV<sup>Sdhb+/-</sup> mice from Dr Louis Maher at the Mayo Clinic (Maher *et al.* 2011) and outbred them to WT C57BL6 mice. Over the ~2-year lifespan study, pheochromocytomas developed in 3 of 44 irradiated *Sdhb+/-* mice and 1 of 10 in irradiated WT mice. However, all of the tumors were *Sdh*-intact by immunohistochemistry and none gave rise to cell lines (previously unpublished data). Cumulatively, our experience suggests that the success of the present project resulted from favorable features of rat biology together with irradiation. However, it is possible that a comparable mouse model might still be developed using mice with a different genetic background or by using a larger number of mice.

In summary, we have developed xenograft and cell line models called RS0 and RS1/2 from PCs that arose in rats with a heterozygous germline mutation in *Sdhb*. RS0 closely recapitulates the genotype and phenotype of hereditary *SDHB*-mutated human PCPG and appears to be a promising model for pre-clinical studies of these tumors. In addition, we identified a carotid body paraganglioma that also appeared to be SDH-deficient based on immunohistochemistry. That tumor was too small to graft or culture and it is possible that additional small paragangliomas were missed amid the large amount of fat in aged rats. This new model may be useful both for pre-clinical drug testing and for basic research aimed at understanding mechanisms involved in the development and progression of SDH-deficient human PCPG.

### Supplementary materials

This is linked to the online version of the paper at <https://doi.org/10.1530/ERC-19-0474>.

### Declaration of interest

The authors declare that there is no conflict of interest that could be perceived as prejudicing the impartiality of the research reported.

### Funding

This research was supported principally by grants to A S T from the SDHB Pheo Para Coalition, the Pheo Para Alliance and the Paradiifference Foundation and by the Intramural Research Program of the Eunice Kennedy Shriver NICHD, NIH. The work utilized NMR instrumentation purchased from a National Institutes of Health SIG grant (S10OD020073). A D P is supported by the Joseph Herman Trust. R W T is supported by a fellowship from the Victorian Cancer Agency.

### Author contribution statement

J P and A T conceived the study, designed the experiments and wrote the manuscript. B C and X Z performed RNA sequencing and analyzed the data. R T and A D P performed whole genome sequencing and analyzed the data. J D B performed metabolomic experiments and analyzed the data. Y O designed the TALEN. I L and A S-B performed immunohistochemical studies. H D S, S J M, T L and K T S contributed to experiments on hypoxic signaling and redox balance. All authors discussed the results and commented on the manuscript.

### Acknowledgements

The authors acknowledge the contribution of Kym Pham and Oliver Hoffman of the University of Melbourne Centre for Cancer Research Genomic and Bioinformatics Platform Groups for their contributions.

## References

- Alexandrov LB, Kim J, Haradhvala NJ, Huang MN, Ng AW, Wu Y, Boot A, Covington KR, Gordenin DA, Bergstrom EN, *et al.* 2019 The repertoire of mutational signatures in human cancer. *Nature* **578** 94–101. (<https://doi.org/10.1038/s41586-020-1943-3>)
- Amar L, Bertherat J, Baudin E, Ajzenberg C, Bressac-de Paillerets B, Chabre O, Chamontin B, Delemer B, Giraud S, Murat A, *et al.* 2005 Genetic testing in pheochromocytoma or functional paraganglioma. *Journal of Clinical Oncology* **23** 8812–8818. (<https://doi.org/10.1200/JCO.2005.03.1484>)
- Amar L, Baudin E, Burnichon N, Peyrard S, Silvera S, Bertherat J, Bertagna X, Schlumberger M, Jeunemaitre X, Gimenez-Roqueplo AP, *et al.* 2007 Succinate dehydrogenase B gene mutations predict survival in patients with malignant pheochromocytomas or paragangliomas. *Journal of Clinical Endocrinology and Metabolism* **92** 3822–3828. (<https://doi.org/10.1210/jc.2007-0709>)
- Bechmann N, Poser I, Seifert V, Greunke C, Ullrich M, Qin N, Walch A, Peitzsch M, Robledo M, Pacak K, *et al.* 2019 Impact of extrinsic and intrinsic hypoxia on catecholamine biosynthesis in absence or presence of Hif2alpha in pheochromocytoma cells. *Cancers* **11** E594. (<https://doi.org/10.3390/cancers11050594>)
- Benn DE, Gimenez-Roqueplo AP, Reilly JR, Bertherat J, Burgess J, Byth K, Croxson M, Dahia PL, Elston M, Gimm O, *et al.* 2006 Clinical presentation and penetrance of pheochromocytoma/paraganglioma syndromes. *Journal of Clinical Endocrinology and Metabolism* **91** 827–836. (<https://doi.org/10.1210/jc.2005-1862>)
- Bezawork-Geleta A, Wen H, Dong L, Yan B, Vider J, Boukalova S, Krobava L, Vanova K, Zobalova R, Sobol M, *et al.* 2018 Alternative assembly of respiratory complex II connects energy stress to metabolic checkpoints. *Nature Communications* **9** 2221. (<https://doi.org/10.1038/s41467-018-04603-z>)
- Blokzijl F, Janssen R, van Boxtel R & Cuppen E 2018 MutationalPatterns: comprehensive genome-wide analysis of mutational processes. *Genome Medicine* **10** 33. (<https://doi.org/10.1186/s13073-018-0539-0>)
- Bolger AM, Lohse M & Usadel B 2014 Trimmomatic: a flexible trimmer for Illumina sequence data. *Bioinformatics* **30** 2114–2120. (<https://doi.org/10.1093/bioinformatics/btu170>)
- Bruntz RC, Lane AN, Higashi RM & Fan TW 2017 Exploring cancer metabolism using stable isotope-resolved metabolomics (SIRM). *Journal of Biological Chemistry* **292** 11601–11609. (<https://doi.org/10.1074/jbc.R117.776054>)
- Burgess MR, Hwang E, Mroue R, Bielski CM, Wandler AM, Huang BJ, Firestone AJ, Young A, Lacap JA, Crocker L, *et al.* 2017 KRAS allelic imbalance enhances fitness and modulates MAP kinase dependence in cancer. *Cell* **168** 817.e15–829.e15. (<https://doi.org/10.1016/j.cell.2017.01.020>)
- Burnichon N, Vescovo L, Amar L, Libe R, de Reynies A, Venisse A, Jouanno E, Laurendeau I, Parfait B, Bertherat J, *et al.* 2011 Integrative genomic analysis reveals somatic mutations in pheochromocytoma and paraganglioma. *Human Molecular Genetics* **20** 3974–3985. (<https://doi.org/10.1093/hmg/ddr324>)
- Cameron DL, Schroder J, Penington JS, Do H, Molania R, Dobrovic A, Speed TP & Papanfuss AT 2017 GRIDSS: sensitive and specific genomic rearrangement detection using positional de Bruijn graph assembly. *Genome Research* **27** 2050–2060. (<https://doi.org/10.1101/gr.222109.117>)
- Carreau A, El Hafny-Rahbi B, Matejuk A, Grillon C & Kieda C 2011 Why is the partial oxygen pressure of human tissues a crucial parameter? Small molecules and hypoxia. *Journal of Cellular and Molecular Medicine* **15** 1239–1253. (<https://doi.org/10.1111/j.1582-4934.2011.01258.x>)
- Castro-Vega LJ, Letouze E, Burnichon N, Buffet A, Disderot PH, Khalifa E, Lorient C, Elarouci N, Morin A, Menara M, *et al.* 2015 Multi-omics analysis defines core genomic alterations in pheochromocytomas and paragangliomas. *Nature Communications* **6** 6044. (<https://doi.org/10.1038/ncomms7044>)
- Cibulskis K, Lawrence MS, Carter SL, Sivachenko A, Jaffe D, Sougnez C, Gabriel S, Meyerson M, Lander ES & Getz G 2013 Sensitive detection of somatic point mutations in impure and heterogeneous cancer samples. *Nature Biotechnology* **31** 213–219. (<https://doi.org/10.1038/nbt.2514>)
- Cogliati S, Enriquez JA & Scorrano L 2016 Mitochondrial cristae: where beauty meets functionality. *Trends in Biochemical Sciences* **41** 261–273. (<https://doi.org/10.1016/j.tibs.2016.01.001>)
- Crona J, Lamarca A, Ghosal S, Welin S, Skogseid B & Pacak K 2019 Genotype-phenotype correlations in pheochromocytoma and paraganglioma. *Endocrine-Related Cancer* **26** 539–550. (<https://doi.org/10.1530/ERC-19-0024>)
- Dahia PLM 2017 Pheochromocytomas and paragangliomas, genetically diverse and minimalist, all at once! *Cancer Cell* **31** 159–161. (<https://doi.org/10.1016/j.ccell.2017.01.009>)
- Dahia PL, Ross KN, Wright ME, Hayashida CY, Santagata S, Barontini M, Kung AL, Sanso G, Powers JF, Tischler AS, *et al.* 2005 A HIF1alpha regulatory loop links hypoxia and mitochondrial signals in pheochromocytomas. *PLoS Genetics* **1** 72–80. (<https://doi.org/10.1371/journal.pgen.0010008>)

- D'Antongiovanni V, Martinelli S, Richter S, Canu L, Guasti D, Mello T, Romagnoli P, Pacak K, Eisenhofer G, Mannelli M, *et al.* 2017 The microenvironment induces collective migration in SDHB-silenced mouse pheochromocytoma spheroids. *Endocrine-Related Cancer* **24** 555–564. (<https://doi.org/10.1530/ERC-17-0212>)
- DePristo MA, Banks E, Poplin R, Garimella KV, Maguire JR, Hartl C, Philippakis AA, del Angel G, Rivas MA, Hanna M, *et al.* 2011 A framework for variation discovery and genotyping using next-generation DNA sequencing data. *Nature Genetics* **43** 491–498. (<https://doi.org/10.1038/ng.806>)
- Didion JP, Martin M & Collins FS 2017 Atropos: specific, sensitive, and speedy trimming of sequencing reads. *PeerJ* **5** e3720. (<https://doi.org/10.7717/peerj.3720>)
- Douwes Dekker PB, Hogendoorn PC, Kuipers-Dijkshoorn N, Prins FA, van Duinen SG, Taschner PE, van der Mey AG & Cornelisse CJ 2003 SDHD mutations in head and neck paragangliomas result in destabilization of complex II in the mitochondrial respiratory chain with loss of enzymatic activity and abnormal mitochondrial morphology. *Journal of Pathology* **201** 480–486. (<https://doi.org/10.1002/path.1461>)
- Durinck S, Moreau Y, Kasprzyk A, Davis S, De Moor B, Brazma A & Huber W 2005 BioMart and Bioconductor: a powerful link between biological databases and microarray data analysis. *Bioinformatics* **21** 3439–3440. (<https://doi.org/10.1093/bioinformatics/bti525>)
- Eischen CM, Weber JD, Roussel MF, Sherr CJ & Cleveland JL 1999 Disruption of the ARF-Mdm2-p53 tumor suppressor pathway in Myc-induced lymphomagenesis. *Genes and Development* **13** 2658–2669. (<https://doi.org/10.1101/gad.13.20.2658>)
- Eisenhofer G, Klink B, Richter S, Lenders JW & Robledo M 2017 Metabologenomics of pheochromocytoma and paraganglioma: an integrated approach for personalised biochemical and genetic testing. *Clinical Biochemist: Reviews* **38** 69–100.
- Favier J, Amar L & Gimenez-Roqueplo AP 2015 Paraganglioma and pheochromocytoma: from genetics to personalized medicine. *Nature Reviews: Endocrinology* **11** 101–111. (<https://doi.org/10.1038/nrendo.2014.188>)
- Favier J, Kempf H, Corvol P & Gasc JM 1999 Cloning and expression pattern of EPAS1 in the chicken embryo. Colocalization with tyrosine hydroxylase. *FEBS Letters* **462** 19–24. ([https://doi.org/10.1016/S0014-5793\(99\)01476-3](https://doi.org/10.1016/S0014-5793(99)01476-3))
- Fishbein L & Wilkerson MD 2018 Chromaffin cell biology: inferences from the Cancer Genome Atlas. *Cell and Tissue Research* **372** 339–346. (<https://doi.org/10.1007/s00441-018-2795-0>)
- Fishbein L, Leshchiner I, Walter V, Danilova L, Robertson AG, Johnson AR, Lichtenberg TM, Murray BA, Ghayee HK, Else T, *et al.* 2017 Comprehensive molecular characterization of pheochromocytoma and paraganglioma. *Cancer Cell* **31** 181–193. (<https://doi.org/10.1016/j.ccell.2017.01.001>)
- Fliedner SM, Breza J, Kvetnansky R, Powers JF, Tischler AS, Wesley R, Merino M, Lehnert H & Pacak K 2010 Tyrosine hydroxylase, chromogranin A, and steroidogenic acute regulator as markers for successful separation of human adrenal medulla. *Cell and Tissue Research* **340** 607–612. (<https://doi.org/10.1007/s00441-010-0965-9>)
- Fliedner SMJ, Brabant G & Lehnert H 2018 Pheochromocytoma and paraganglioma: genotype versus anatomic location as determinants of tumor phenotype. *Cell and Tissue Research* **372** 347–365. (<https://doi.org/10.1007/s00441-017-2760-3>)
- Flynn A, Benn D, Clifton-Bligh R, Robinson B, Trainer AH, James P, Hogg A, Waldeck K, George J, Li J, *et al.* 2015 The genomic landscape of pheochromocytoma. *Journal of Pathology* **236** 78–89. (<https://doi.org/10.1002/path.4503>)
- Greene LA & Tischler AS 1976 Establishment of a noradrenergic clonal line of rat adrenal pheochromocytoma cells which respond to nerve growth factor. *PNAS* **73** 2424–2428. (<https://doi.org/10.1073/pnas.73.7.2424>)
- Gu Z, Gu L, Eils R, Schlesner M & Brors B 2014 Circlize implements and enhances circular visualization in R. *Bioinformatics* **30** 2811–2812. (<https://doi.org/10.1093/bioinformatics/btu393>)
- Hall LB, Yoshitomi K & Boorman GA 1987 Pathologic features of abdominal and thoracic paragangliomas in F344/N rats. *Veterinary Pathology* **24** 315–322. (<https://doi.org/10.1177/030098588702400405>)
- Hammarlund EU, von Stedingk K & Pahlman S 2018 Refined control of cell stemness allowed animal evolution in the oxic realm. *Nature Ecology and Evolution* **2** 220–228. (<https://doi.org/10.1038/s41559-017-0410-5>)
- Hawes JJ, Tuskan RG & Reilly KM 2007 Nf1 expression is dependent on strain background: implications for tumor suppressor haploinsufficiency studies. *Neurogenetics* **8** 121–130. (<https://doi.org/10.1007/s10048-006-0078-5>)
- Hescot S, Curras-Freixes M, Deutschbein T, van Berkel A, Vezzosi D, Amar L, de la Fouchardiere C, Valdes N, Riccardi F, Do Cao C, *et al.* 2019 Prognosis of malignant pheochromocytoma and paraganglioma (MAPP-Prono study): a European Network for the Study of Adrenal Tumors retrospective study. *Journal of Clinical Endocrinology and Metabolism* **104** 2367–2374. (<https://doi.org/10.1210/jc.2018-01968>)
- Jacks T, Shih TS, Schmitt EM, Bronson RT, Bernards A & Weinberg RA 1994 Tumour predisposition in mice heterozygous for a targeted mutation in Nf1. *Nature Genetics* **7** 353–361. (<https://doi.org/10.1038/ng0794-353>)
- Jochmanova I, Wolf KI, King KS, Nambuba J, Wesley R, Martucci V, Raygada M, Adams KT, Prodanov T, Fojo AT, *et al.* 2017 SDHB-related pheochromocytoma and paraganglioma penetrance and genotype-phenotype correlations. *Journal of Cancer Research and Clinical Oncology* **143** 1421–1435. (<https://doi.org/10.1007/s00432-017-2397-3>)
- Kim D, Pertea G, Trapnell C, Pimentel H, Kelley R & Salzberg SL 2013 TopHat2: accurate alignment of transcriptomes in the presence of insertions, deletions and gene fusions. *Genome Biology* **14** R36. (<https://doi.org/10.1186/gb-2013-14-4-r36>)
- Kim S, Scheffler K, Halpern AL, Bekritsky MA, Noh E, Kallberg M, Chen X, Kim Y, Beyter D, Krusche P, *et al.* 2018 Strelka2: fast and accurate calling of germline and somatic variants. *Nature Methods* **15** 591–594. (<https://doi.org/10.1038/s41592-018-0051-x>)
- Kiss NB, Geli J, Lundberg F, Avci C, Velazquez-Fernandez D, Hashemi J, Weber G, Hoog A, Ekstrom TJ, Backdahl M, *et al.* 2008 Methylation of the p16INK4A promoter is associated with malignant behavior in abdominal extra-adrenal paragangliomas but not pheochromocytomas. *Endocrine-Related Cancer* **15** 609–621. (<https://doi.org/10.1677/ERC-07-0285>)
- Kluckova K, Thakker A, Vettore L, Escobedo-Gonzalez C, Hindshaw RL, Tearle JLE, Goncalves J, Kaul B, Lavery GG, Favier J, *et al.* 2020 Succinate dehydrogenase deficiency in a chromaffin cell model retains metabolic fitness through the maintenance of mitochondrial NADH oxidoreductase function. *FASEB Journal* **34** 303–315. (<https://doi.org/10.1096/fj.201901456R>)
- Koboldt DC, Zhang Q, Larson DE, Shen D, McLellan MD, Lin L, Miller CA, Mardis ER, Ding L & Wilson RK 2012 VarScan 2: somatic mutation and copy number alteration discovery in cancer by exome sequencing. *Genome Research* **22** 568–576. (<https://doi.org/10.1101/gr.129684.111>)
- Korpershoek E, Favier J, Gaal J, Burnichon N, van Gessel B, Oudijk L, Badoual C, Gadessaud N, Venisse A, Bayley JP, *et al.* 2011 SDHA immunohistochemistry detects germline SDHA gene mutations in apparently sporadic paragangliomas and pheochromocytomas. *Journal of Clinical Endocrinology and Metabolism* **96** E1472–E1476. (<https://doi.org/10.1210/jc.2011-1043>)
- Korpershoek E, Petri BJ, Post E, van Eijck CH, Oldenburg RA, Belt EJ, de Herder WW, de Krijger RR & Dinjens WN 2014 Adrenal medullary hyperplasia is a precursor lesion for pheochromocytoma in MEN2

- syndrome. *Neoplasia* **16** 868–873. (<https://doi.org/10.1016/j.neo.2014.09.002>)
- Letouze E, Martinelli C, Lorient C, Burnichon N, Abermil N, Ottolenghi C, Janin M, Menara M, Nguyen AT, Benit P, *et al.* 2013 SDH mutations establish a hypermethylator phenotype in paraganglioma. *Cancer Cell* **23** 739–752. (<https://doi.org/10.1016/j.ccr.2013.04.018>)
- Li H 2013 Aligning sequence reads, clone sequences and assembly contigs with BWA-MEM. *arXiv* 1303.3997. (available at: <https://arxiv.org/abs/1303.3997>)
- Li Y, Shiraiwa K, Ko KN, Moon J, Park SH, Lee M, Shin S, Kim M, Jang H, Lee Y, *et al.* 2013 A paraganglioma in the posterior wall of the left atrium originating from the aortic body in a Wistar Hannover rat. *Experimental and Toxicologic Pathology* **65** 631–636. (<https://doi.org/10.1016/j.etp.2012.07.002>)
- Liao Y, Smyth GK & Shi W 2014 featureCounts: an efficient general purpose program for assigning sequence reads to genomic features. *Bioinformatics* **30** 923–930. (<https://doi.org/10.1093/bioinformatics/btt656>)
- Lloyd R, Osamura R, Klöppel G & Rosai J 2017 *WHO Classification of Tumours of Endocrine Organs*, 4th ed. Lyon, France: IARC Press.
- Lussey-Lepoutre C, Hollinshead KE, Ludwig C, Menara M, Morin A, Castro-Vega LJ, Parker SJ, Janin M, Martinelli C, Ottolenghi C, *et al.* 2015 Loss of succinate dehydrogenase activity results in dependency on pyruvate carboxylation for cellular anabolism. *Nature Communications* **6** 8784. (<https://doi.org/10.1038/ncomms9784>)
- Lussey-Lepoutre C, Buffet A, Morin A, Goncalves J & Favier J 2018 Rodent models of pheochromocytoma, parallels in rodent and human tumorigenesis. *Cell and Tissue Research* **372** 379–392. (<https://doi.org/10.1007/s00441-018-2797-y>)
- Maher LJI, Smith EH, Rueter EM, Becker NA, Bida JP, Nelson-Holte M, Palomo JIP, García-Flores P, López-Barneo J & van Deusen J 2011 Mouse models of human familial paraganglioma. In *Pheochromocytoma – A New View of the Old Problem*. Ed JF Martin. London, UK: InTech. (<https://doi.org/10.5772/25346>)
- McKenna A, Hanna M, Banks E, Sivachenko A, Cibulskis K, Kernytzky A, Garimella K, Altshuler D, Gabriel S, Daly M, *et al.* 2010 The Genome Analysis Toolkit: a MapReduce framework for analyzing next-generation DNA sequencing data. *Genome Research* **20** 1297–1303. (<https://doi.org/10.1101/gr.107524.110>)
- Merkert S & Martin U 2018 Targeted gene editing in human pluripotent stem cells using site-specific nucleases. *Advances in Biochemical Engineering/Biotechnology* **163** 169–186. ([https://doi.org/10.1007/10\\_2017\\_25](https://doi.org/10.1007/10_2017_25))
- Mermel CH, Schumacher SE, Hill B, Meyerson ML, Beroukhir R & Getz G 2011 GISTIC2.0 facilitates sensitive and confident localization of the targets of focal somatic copy-number alteration in human cancers. *Genome Biology* **12** R41. (<https://doi.org/10.1186/gb-2011-12-4-r41>)
- Muir A & Vander Heiden MG 2018 The nutrient environment affects therapy. *Science* **360** 962–963. (<https://doi.org/10.1126/science.aar5986>)
- Muscarella P, Bloomston M, Brewer AR, Mahajan A, Frankel WL, Ellison EC, Farrar WB, Weghorst CM & Li J 2008 Expression of the p16INK4A/Cdkn2a gene is prevalently downregulated in human pheochromocytoma tumor specimens. *Gene Expression* **14** 207–216. (<https://doi.org/10.3727/105221608786883825>)
- Pace V, Perentes E & Germann PG 2002 Pheochromocytomas and ganglioneuromas in the aging rats: morphological and immunohistochemical characterization. *Toxicologic Pathology* **30** 492–500. (<https://doi.org/10.1080/01926230290105668>)
- Pang Y, Lu Y, Caisova V, Liu Y, Bullova P, Huynh TT, Zhou Y, Yu D, Frysak Z, Hartmann I, *et al.* 2018 Targeting NAD(+)/PARP DNA repair pathway as a novel therapeutic approach to SDHB-mutated cluster I pheochromocytoma and paraganglioma. *Clinical Cancer Research* **24** 3423–3432. (<https://doi.org/10.1158/1078-0432.CCR-17-3406>)
- Papathomas TG, Oudijk L, Persu A, Gill AJ, van Nederveen F, Tischler AS, Tissier F, Volante M, Matias-Guiu X, Smid M, *et al.* 2015 SDHB/SDHA immunohistochemistry in pheochromocytomas and paragangliomas: a multicenter interobserver variation analysis using virtual microscopy: a Multinational Study of the European Network for the Study of Adrenal Tumors (ENS@T). *Modern Pathology* **28** 807–821. (<https://doi.org/10.1038/modpathol.2015.41>)
- Pasini B & Stratakis CA 2009 SDH mutations in tumorigenesis and inherited endocrine tumours: lesson from the pheochromocytoma-paraganglioma syndromes. *Journal of Internal Medicine* **266** 19–42. (<https://doi.org/10.1111/j.1365-2796.2009.02111.x>)
- Persson CU, von Stedingk K, Bexell D, Merselius M, Braekvelde N, Gisselsson D, Arsenian-Henriksson M, Pahlman S & Wigerup C 2017 Neuroblastoma patient-derived xenograft cells cultured in stem-cell promoting medium retain tumorigenic and metastatic capacities but differentiate in serum. *Scientific Reports* **7** 10274. (<https://doi.org/10.1038/s41598-017-09662-8>)
- Piruat JI, Pintado CO, Ortega-Saenz P, Roche M & Lopez-Barneo J 2004 The mitochondrial SDHD gene is required for early embryogenesis, and its partial deficiency results in persistent carotid body glomus cell activation with full responsiveness to hypoxia. *Molecular and Cellular Biology* **24** 10933–10940. (<https://doi.org/10.1128/MCB.24.24.10933-10940.2004>)
- Powers JF, Evinger MJ, Tsokas P, Bedri S, Alroy J, Shahsavari M & Tischler AS 2000 Pheochromocytoma cell lines from heterozygous neurofibromatosis knockout mice. *Cell and Tissue Research* **302** 309–320. (<https://doi.org/10.1007/s004410000290>)
- Powers JF, Picard KL & Tischler AS 2009 RET expression and neuron-like differentiation of pheochromocytoma and normal chromaffin cells. *Hormone and Metabolic Research* **41** 710–714. (<https://doi.org/10.1055/s-0029-1224136>)
- Powers JF, Pacak K & Tischler AS 2017 Pathology of human pheochromocytoma and paraganglioma xenografts in NSG mice. *Endocrine Pathology* **28** 2–6. (<https://doi.org/10.1007/s12022-016-9452-5>)
- Powers JF, Cochran B, Baleja JD, Sikes HD, Zhang X, Lomakin I, Langford T, Stein KT & Tischler AS 2018 A unique model for SDH-deficient GIST: an endocrine-related cancer. *Endocrine-Related Cancer* **25** 943–954. (<https://doi.org/10.1530/ERC-18-0115>)
- Raney BJ, Dreszer TR, Barber GP, Clawson H, Fujita PA, Wang T, Nguyen N, Paten B, Zweig AS, Karolchik D, *et al.* 2014 Track data hubs enable visualization of user-defined genome-wide annotations on the UCSC Genome Browser. *Bioinformatics* **30** 1003–1005. (<https://doi.org/10.1093/bioinformatics/btt637>)
- Richter S, Qin N, Pacak K & Eisenhofer G 2013 Role of hypoxia and HIF2 $\alpha$  in development of the sympathoadrenal cell lineage and chromaffin cell tumors with distinct catecholamine phenotypic features. *Advances in Pharmacology* **68** 285–317. (<https://doi.org/10.1016/B978-0-12-411512-5.00014-2>)
- Richter S, Peitzsch M, Rapizzi E, Lenders JW, Qin N, de Cubas AA, Schiavi F, Rao JU, Beuschlein F, Quinkler M, *et al.* 2014 Krebs cycle metabolite profiling for identification and stratification of pheochromocytomas/paragangliomas due to succinate dehydrogenase deficiency. *Journal of Clinical Endocrinology and Metabolism* **99** 3903–3911. (<https://doi.org/10.1210/jc.2014-2151>)
- Rijken JA, Niemeijer ND, Jonker MA, Eijkelenkamp K, Jansen JC, van Berkel A, Timmers HJLM, Kunst HPM, Bisschop P, Kerstens MN, *et al.* 2017 The penetrance of paraganglioma and pheochromocytoma in SDHB germline mutation carriers. *Clinical Genetics* **93** 60–66. (<https://doi.org/10.1111/cge.13055>)
- Robinson MD, McCarthy DJ & Smyth GK 2010 edgeR: a Bioconductor package for differential expression analysis of digital gene expression data. *Bioinformatics* **26** 139–140. (<https://doi.org/10.1093/bioinformatics/btp616>)

- Robinson JT, Thorvaldsdottir H, Winckler W, Guttman M, Lander ES, Getz G & Mesirov JP 2011 Integrative genomics viewer. *Nature Biotechnology* **29** 24–26. (<https://doi.org/10.1038/nbt.1754>)
- Shultz LD, Goodwin N, Ishikawa F, Hosur V, Lyons BL & Greiner DL 2014 Human cancer growth and therapy in immunodeficient mouse models. *Cold Spring Harbor Protocols* **2014** 694–708. (<https://doi.org/10.1101/pdb.top073585>)
- Szarek E, Ball ER, Imperiale A, Tsokos M, Faucz FR, Giubellino A, Moussallieh FM, Namer IJ, Abu-Asab MS, Pacak K, *et al.* 2015 Carney triad, SDH-deficient tumors, and *Sdhb*+/- mice share abnormal mitochondria. *Endocrine-Related Cancer* **22** 345–352. (<https://doi.org/10.1530/ERC-15-0069>)
- Tate JG, Bamford S, Jubb HC, Sondka Z, Beare DM, Bindal N, Boutselakis H, Cole CG, Creatore C, Dawson E, *et al.* 2019 COSMIC: the catalogue of somatic mutations in cancer. *Nucleic Acids Research* **47** D941–D947. (<https://doi.org/10.1093/nar/gky1015>)
- Tella SH, Taieb D & Pacak K 2017 HIF-2alpha: Achilles' heel of pseudohypoxic subtype paraganglioma and other related conditions. *European Journal of Cancer* **86** 1–4. (<https://doi.org/10.1016/j.ejca.2017.08.023>)
- Tischler AS & deKrijger RR 2015 15 YEARS OF PARAGANGLIOMA: Pathology of pheochromocytoma and paraganglioma. *Endocrine-Related Cancer* **22** T123–T133. (<https://doi.org/10.1530/ERC-15-0261>)
- Tischler AS, Ruzicka LA & Riseberg JC 1992 Immunocytochemical analysis of chromaffin cell proliferation in vitro. *Journal of Histochemistry and Cytochemistry* **40** 1043–1045. (<https://doi.org/10.1177/40.7.1351491>)
- Tischler AS, Riseberg JC & Cherington V 1994 Multiple mitogenic signalling pathways in chromaffin cells: a model for cell cycle regulation in the nervous system. *Neuroscience Letters* **168** 181–184. ([https://doi.org/10.1016/0304-3940\(94\)90445-6](https://doi.org/10.1016/0304-3940(94)90445-6))
- Tischler AS, Shih TS, Williams BO & Jacks T 1995 Characterization of pheochromocytomas in a mouse strain with a targeted disruptive mutation of the neurofibromatosis gene *Nf1*. *Endocrine Pathology* **6** 323–335. (<https://doi.org/10.1007/bf02738732>)
- Tischler AS, Powers JF & Alroy J 2004 Animal models of pheochromocytoma. *Histology and Histopathology* **19** 883–895. (<https://doi.org/10.14670/HH-19.883>)
- Tischler AS, Nyska A & Elmore SA 2014 Toxic responses of the adrenal medulla. In *Reference Module in Biomedical Sciences*. Amsterdam, Netherlands: Elsevier. (<https://doi.org/10.1016/B978-0-12-801238-3.02146-2>)
- van Nederveen FH, Gaal J, Favier J, Korpershoek E, Oldenburg RA, de Bruyn EM, Sleddens HF, Derckx P, Riviere J, Dannenberg H, *et al.* 2009 An immunohistochemical procedure to detect patients with paraganglioma and pheochromocytoma with germline SDHB, SDHC, or SDHD gene mutations: a retrospective and prospective analysis. *Lancet: Oncology* **10** 764–771. ([https://doi.org/10.1016/S1470-2045\(09\)70164-0](https://doi.org/10.1016/S1470-2045(09)70164-0))
- van Zwieten MJ, Burek JD, Zurcher C & Hollander CF 1979 Aortic body tumours and hyperplasia in the rat. *Journal of Pathology* **128** 99–112. (<https://doi.org/10.1002/path.1711280208>)
- Warren S & Chute RN 1972 Pheochromocytoma. *Cancer* **29** 327–331. ([https://doi.org/10.1002/1097-0142\(197202\)29:2<327::aid-cncr2820290210>3.0.co;2-3](https://doi.org/10.1002/1097-0142(197202)29:2<327::aid-cncr2820290210>3.0.co;2-3))
- Wilkerson MD & Hayes DN 2010 ConsensusClusterPlus: a class discovery tool with confidence assessments and item tracking. *Bioinformatics* **26** 1572–1573. (<https://doi.org/10.1093/bioinformatics/btq170>)
- Zerbino DR, Achuthan P, Akanni W, Amode MR, Barrell D, Bhai J, Billis K, Cummins C, Gall A, Giron CG, *et al.* 2018 Ensembl 2018. *Nucleic Acids Research* **46** D754–D761. (<https://doi.org/10.1093/nar/gkx1098>)

Received in final form 31 March 2020

Accepted 3 April 2020

Accepted Manuscript published online 3 April 2020

## ERRATUM

# A xenograft and cell line model of SDH-deficient pheochromocytoma derived from *Sdhb*<sup>+/-</sup> rats

James F Powers<sup>1</sup>, Brent Cochran<sup>2</sup>, James D Baleja<sup>2</sup>, Hadley D Sikes<sup>3</sup>, Andrew D Pattison<sup>4</sup>, Xue Zhang<sup>2</sup>, Inna Lomakin<sup>1</sup>, Annette Shepard-Barry<sup>1</sup>, Karel Pacak<sup>5</sup>, Sun Jin Moon<sup>3</sup>, Troy F Langford<sup>3</sup>, Kassi Taylor Stein<sup>6</sup>, Richard W Tothill<sup>4,6</sup>, Yingbin Ouyang<sup>7</sup> and Arthur S Tischler<sup>1</sup>

<sup>1</sup>Department of Pathology and Laboratory Medicine, Tufts Medical Center, Tufts University School of Medicine, Boston, Massachusetts, USA

<sup>2</sup>Department of Developmental, Molecular and Chemical Biology, Tufts University School of Medicine, Boston, Massachusetts, USA

<sup>3</sup>Department of Chemical Engineering, Massachusetts Institute of Technology, Cambridge, Massachusetts, USA

<sup>4</sup>Department of Clinical Pathology, University of Melbourne, Melbourne, Victoria, Australia

<sup>5</sup>Section on Medical Neuroendocrinology, Eunice Kennedy Shriver Division National Institute of Child Health and Human Development, Bethesda, Maryland, USA

<sup>6</sup>Peter MacCallum Cancer Centre, Melbourne, Victoria, Australia

<sup>7</sup>Cyagen US Inc, Santa Clara, California, USA

Correspondence should be addressed to J F Powers: [jpowers1@tuftsmedicalcenter.org](mailto:jpowers1@tuftsmedicalcenter.org)

*Endocrine-Related Cancer*  
(2020) **27**, X9–X10

The authors and journal apologise for an error in the above paper, which appeared in volume 27 part 6, pages 337–354. The error relates to the artwork of Table 1 on page 346, in which the units were given in micromoles per milligram of tissue, when the units should have been given in nanomoles per milligram of tissue.

The correct Table 1 is given in full below:

**Table 1** NMR metabolomic profiles of RS0, RS1/2 xenografts and rat adrenal medulla (RAM).

RAM (20 pooled)	RS0 (n = 4)		RS1/2 (n = 3)	
	Mean ± s.e.m.	Mean ± s.e.m.	Mean ± s.e.m.	Mean ± s.e.m.
The 10 most abundant detectable metabolites (nmol/mg of tissue)				
Epinephrine	16.15	15.18 ± 3.66	Norepinephrine	33.87 ± 29.41
Norepinephrine	12.33	12.11 ± 2.69	Lactate	11.45 ± 2.18
Glucose	2.31	5.99 ± 1.19	Taurine	10.38 ± 0.83
Lactate	0.89	3.47 ± 0.75	Ascorbate	7.611 ± .42
Taurine	0.61	2.57 ± 0.58	myo-Inositol	6.33 ± 2.80
ATP (or ADP)	0.59	2.57 ± 0.64	Glutamate	4.16 ± 0.97
Ascorbate	0.44	2.08 ± 0.45	Dopamine	2.55 ± 2.04
AMP	0.30	1.39 ± 0.28	O-Phosphoethanolamine	2.06 ± 0.25
ADP (or ATP)	0.21	1.29 ± 0.34	AMP	1.85 ± 1.39
Glutamate	0.17	1.21 ± 0.26	Betaine	1.83 ± 0.31
<b>Succinate</b>			<b>Succinate</b>	
30 of 67	0.01		30 of 67	0.29 ± 0.10
Catecholamine and metabolite profile (nmol/mg of tissue)				
Dopamine	0.07	0.38 ± 0.08		2.55 ± 2.04
3,4-Dihydroxybenzeneacetate <sup>a</sup>	0.00	0.05 ± 0.02		0.23 ± 0.05
Norepinephrine	12.33	0.06 ± 0.03		33.87 ± 29.41
Normetanephrine	0.00	0.02 ± 0.01		0.00 ± 0.00
Epinephrine	16.15	0.00 ± 0.00		0.81 ± 0.78
Tyrosine	0.00	0.11 ± 0.01		0.03 ± 0.00

<sup>a</sup>3,4 dihydroxyphenylacetic acid (DOPAC).



Published in final edited form as:

*Metabolism*. 2020 September ; 110: 154297. doi:10.1016/j.metabol.2020.154297.

## Targeting pheochromocytoma/paraganglioma with polyamine inhibitors

Sudhir Kumar Rai<sup>a,1</sup>, Fernando Bril<sup>b,1</sup>, Heather M. Hatch<sup>c</sup>, Yiling Xu<sup>a</sup>, Laura Shelton<sup>d</sup>, Srilaxmi Kalavalapalli<sup>a</sup>, Arielle Click<sup>e</sup>, Douglas Lee<sup>f</sup>, Chris Beecher<sup>g</sup>, Austin Kirby<sup>h</sup>, Kimi Kong<sup>h</sup>, Jose Trevino<sup>i</sup>, Abhishek Jha<sup>j</sup>, Shashank Jatav<sup>j</sup>, Kriti Kriti<sup>j</sup>, Soumya Luthra<sup>j</sup>, Timothy J. Garrett<sup>k</sup>, Joy Guingab-Cagmat<sup>k</sup>, Daniel Plant<sup>l</sup>, Prodip Bose<sup>l</sup>, Kenneth Cusi<sup>p</sup>, Robert A. Hromas<sup>h</sup>, Arthur S. Tischler<sup>m</sup>, James F. Powers<sup>m</sup>, Priyanka Gupta<sup>n</sup>, James Bibb<sup>n</sup>, Felix Beuschlein<sup>o</sup>, Mercedes Robledo<sup>p</sup>, Bruna Calsina<sup>p</sup>, Henri Timmers<sup>q</sup>, David Taieb<sup>r</sup>, Matthias Kroiss<sup>s</sup>, Susan Richter<sup>t</sup>, Katharina Langton<sup>u</sup>, Graeme Eisenhofer<sup>t,u,v</sup>, Raymond Bergeron Jr.<sup>w</sup>, Karel Pacak<sup>x</sup>, Sergei G. Tevosian<sup>c,\*</sup>, Hans K. Ghayee<sup>b,\*</sup>

<sup>a</sup>Department of Medicine, Division of Endocrinology, University of Florida, Gainesville, FL, USA

<sup>b</sup>Department of Medicine, Division of Endocrinology, University of Florida and Malcom Randall VA Medical Center, Gainesville, FL, USA

<sup>c</sup>Department of Physiological Sciences, University of Florida, Gainesville, FL, USA

<sup>d</sup>Scientific Project Development, Human Metabolome Technologies, Boston, MA, USA

<sup>e</sup>Department of Immunology, University of Texas Southwestern Medical Center, Dallas, TX, USA

<sup>f</sup>Omic Insight, LLC, Durham, NC, USA

<sup>g</sup>IROA Technologies, Chapel Hill, NC, USA

<sup>h</sup>Department of Medicine, University of Texas Health Science Center, San Antonio, TX, USA

<sup>i</sup>Department of Surgery, University of Florida, Gainesville, FL, USA

<sup>j</sup>Elucidata, Cambridge, MA, USA

<sup>k</sup>Department of Pathology, Immunology, and Laboratory Medicine, University of Florida, Gainesville, FL, USA

<sup>l</sup>Department of Physiological Sciences, University of Florida, Malcom Randall VA Medical Center, Gainesville, FL, USA

<sup>m</sup>Department of Pathology and Laboratory Medicine, Tufts Medical Center, Boston, MA, USA

<sup>n</sup>Department of Surgery, University of Florida

<sup>o</sup>Department of Surgery, University of Florida

<sup>p</sup>Department of Surgery, University of Florida

<sup>q</sup>Department of Surgery, University of Florida

<sup>r</sup>Department of Surgery, University of Florida

<sup>s</sup>Department of Surgery, University of Florida

<sup>t</sup>Department of Surgery, University of Florida

<sup>u</sup>Department of Surgery, University of Florida

<sup>v</sup>Department of Surgery, University of Florida

<sup>w</sup>Department of Surgery, University of Florida

<sup>x</sup>Department of Surgery, University of Florida

<sup>y</sup>Department of Surgery, University of Florida

<sup>z</sup>Department of Surgery, University of Florida

<sup>aa</sup>Department of Surgery, University of Florida

<sup>ab</sup>Department of Surgery, University of Florida

<sup>ac</sup>Department of Surgery, University of Florida

<sup>ad</sup>Department of Surgery, University of Florida

<sup>ae</sup>Department of Surgery, University of Florida

<sup>af</sup>Department of Surgery, University of Florida

<sup>ag</sup>Department of Surgery, University of Florida

<sup>ah</sup>Department of Surgery, University of Florida

<sup>ai</sup>Department of Surgery, University of Florida

<sup>aj</sup>Department of Surgery, University of Florida

<sup>ak</sup>Department of Surgery, University of Florida

<sup>al</sup>Department of Surgery, University of Florida

<sup>am</sup>Department of Surgery, University of Florida

<sup>an</sup>Department of Surgery, University of Florida

<sup>ao</sup>Department of Surgery, University of Florida

<sup>ap</sup>Department of Surgery, University of Florida

\*Correspondence to: S.G. Tevosian, Department of Physiological Sciences, University of Florida, Gainesville, FL 32610, USA.

\*\*Correspondence to: H.K. Ghayee, Division of Endocrinology, University of Florida and Malcom Randall VA Medical Center, Gainesville, FL 32610, USA. stevosian@ufl.edu (S.G. Tevosian), hans.ghayee@medicine.ufl.edu (H.K. Ghayee).

<sup>1</sup>Authors contributed equally.

CRedit authorship contribution statement

**Sudhir Kumar Rai**:Methodology, Investigation, Writing - original draft.**Fernando Bril**:Methodology, Formal analysis, Investigation, Resources, Writing - original draft.**Heather M. Hatch**:Methodology, Investigation.**Yiling Xu**:Methodology, Investigation.**Laura Shelton**:Formal analysis, Investigation.**Srilaxmi Kalavalapalli**:Methodology, Formal analysis, Investigation.**Arielle Click**:Investigation.**Douglas Lee**:Investigation.**Chris Beecher**:Investigation.**Austin Kirby**:Investigation.**Kimi Kong**:Formal analysis.**Jose Trevino**:Methodology.**Abhishek Jha**:Formal analysis.**Shashank Jatav**:Formal analysis.**Kriti Kriti**:Funding acquisition.**Soumya Luthra**:Formal analysis.**Timothy J. Garrett**:Investigation.**Joy Guingab-Cagmat**:Investigation.**Daniel Plant**:Investigation.**Prodip Bose**:Investigation.**Kenneth Cusi**:Resources, Funding acquisition.**Robert A. Hromas**:Conceptualization, Resources, Funding acquisition.**Arthur S. Tischler**:Resources.**James F. Powers**:Resources.**Priyanka Gupta**:Resources.**James Bibb**:Resources.**Felix Beuschlein**:Methodology, Formal analysis, Investigation, Resources, Writing - original draft.**Mercedes Robledo**:Resources.**Bruna Calsina**:Resources.**Henri Timmers**:Resources.**David Taieb**:Resources.**Matthias Kroiss**:Resources.**Susan Richter**:Resources.**Katharina Langton**:Resources.**Graeme Eisenhofer**:Conceptualization, Resources, Project administration.**Raymond Bergeron**:Conceptualization, Resources.**Karel Pacak**:Conceptualization, Resources.**Sergei G. Tevosian**:Conceptualization, Resources, Writing - original draft, Project administration.**Hans K. Ghayee**:Conceptualization, Writing - original draft, Project administration, Funding acquisition.

Supplementary data to this article can be found online at <https://doi.org/10.1016/j.metabol.2020.154297>.

Declaration of competing interest

R.B. invented the polyamine drug platforms and holds a number of patents in polyamine drug development. H.K.G. received royalties from the University of Texas Southwestern Medical Center at Dallas.

Alabama, Birmingham, AL, USA <sup>o</sup>Klinik für Endokrinologie, Diabetologie und Klinische Ernährung, UniversitätsSpital Zurich, Zurich, Switzerland <sup>p</sup>Hereditary Endocrine Cancer Group, Spanish National Cancer Research Center (CNIO), and Centro de Investigación Biomédica en Red de Enfermedades Raras (CIBERER), Madrid, Spain <sup>q</sup>Department of Internal Medicine, Radboud University Medical Center, Nijmegen, Netherlands <sup>r</sup>Department of Nuclear Medicine, La Timone University Hospital, European Center for Research in Medical Imaging, Aix Marseille Université, Marseille, France <sup>s</sup>Department of Internal Medicine, Division of Endocrinology and Diabetology, University Hospital Würzburg, University of Würzburg Würzburg, Germany <sup>t</sup>Institute of Clinical Chemistry and Laboratory Medicine, University Hospital Carl Gustav Carus, Technische Universität Dresden, Germany <sup>u</sup>Department of Medicine III, University Hospital Carl Gustav Carus, Technische Universität Dresden, Germany <sup>v</sup>Division of Clinical Neurochemistry, Institute of Clinical Chemistry and Laboratory Medicine, and Department of Medicine, Faculty of Medicine, University Hospital Carl Gustav Carus, Technische Universität Dresden, Germany <sup>w</sup>Department of Medicinal Chemistry, University of Florida, Gainesville, FL, USA <sup>x</sup>Eunice Kennedy Shriver National Institute of Child Health and Human Development, National Institutes of Health, Bethesda, MD, USA

## Abstract

**Background:** Pheochromocytomas (PCCs) and paragangliomas (PGLs) are neuroendocrine tumors that are mostly benign. Metastatic disease does occur in about 10% of cases of PCC and up to 25% of PGL, and for these patients no effective therapies are available. Patients with mutations in the succinate dehydrogenase subunit B (*SDHB*) gene tend to have metastatic disease. We hypothesized that a down-regulation in the active succinate dehydrogenase B subunit should result in notable changes in cellular metabolic profile and could present a vulnerability point for successful pharmacological targeting.

**Methods:** Metabolomic analysis was performed on human hPheo1 cells and shRNA *SDHB* knockdown hPheo1 (hPheo1 *SDHB* KD) cells. Additional analysis of 115 human fresh frozen samples was conducted. In vitro studies using *N*<sup>1</sup>,*N*<sup>1</sup>-diethylnorspermine (DENS PM) and *N*<sup>1</sup>,*N*<sup>12</sup>-diethylspermine (DESPM) treatments were carried out. DENS PM efficacy was assessed in human cell line derived mouse xenografts.

**Results:** Components of the polyamine pathway were elevated in hPheo1 *SDHB* KD cells compared to wild-type cells. A similar observation was noted in *SDHx* PCC/PGLs tissues compared to their non-mutated counterparts. Specifically, spermidine, and spermine were significantly elevated in *SDHx*-mutated PCC/PGLs, with a similar trend in hPheo1 *SDHB* KD cells. Polyamine pathway inhibitors DENS PM and DESPM effectively inhibited growth of hPheo1 cells in vitro as well in mouse xenografts.

**Conclusions:** This study demonstrates overactive polyamine pathway in PCC/PGL with *SDHB* mutations. Treatment with polyamine pathway inhibitors significantly inhibited hPheo1 cell growth and led to growth suppression in xenograft mice treated with DENS PM. These studies strongly implicate the polyamine pathway in PCC/PGL pathophysiology and provide new foundation for exploring the role for polyamine analogue inhibitors in treating metastatic PCC/PGL.

## Précis:

Cell line metabolomics on hPheo1 cells and PCC/PGL tumor tissue indicate that the polyamine pathway is activated. Polyamine inhibitors in vitro and in vivo demonstrate that polyamine inhibitors are promising for malignant PCC/PGL treatment. However, further research is warranted.

## Keywords

Polyamine; Pheochromocytoma (PCC); Paranglioma (PGL); *SDHB*; DENS PM; DES PM

---

## 1. Introduction

Pheochromocytomas (PCC) and paragangliomas (PGL) are catecholamine-producing tumors derived from chromaffin cells of the adrenal medulla and sympathetic/parasympathetic chain ganglia, respectively. Patients afflicted with metastatic PCC/PGLs have a <40% 5 year survival rate [1-3]. Hypertension and palpitations are the usual presenting symptoms, and devastating complications of excess catecholamine levels including cardiovascular collapse have been documented [4]. Surgical removal is the only definitive treatment, as reliable medical therapies to control tumor growth or metastatic lesions are limited [5,6].

Despite major advances in understanding the genetic landscape of hereditary PCC/PGL syndromes, the biochemical mechanisms regulating growth and metastasis in these neuroendocrine tumors remain obscure and druggable targets have yet to emerge. The Cancer Genome Atlas (TCGA) consortium published the most comprehensive study of PCC/PGLs through multimodal genomic profiling in the largest assortment of tumors collected internationally, with standardized quality control and internally reviewed histopathology [7]. This work solidified a classification of PCC/PGL that includes independent tumor groups based on their profiling. Cluster 1 includes the hypoxia pathway associated tumors (with mutations in *VHL* and *SDHx*). Cluster 2 includes tumors associated with kinase signaling pathway (with mutations in *RET*, *NF-1*, and *TMEM127*). Cluster 3 is composed of tumors carrying the Mastermind-like 3 (MAML-3) mutations [7-11].

The gene most closely associated with metastatic tumor behavior is the succinate dehydrogenase complex iron sulfur subunit B gene (*SDHB*) that belongs to Cluster I [12-14]. *SDHB* is a subunit of a key Krebs cycle enzyme, succinate dehydrogenase, that is involved in conversion of succinate to fumarate [15,16]. Mutations in the *SDHx* genes are associated with accumulation of various intermediate metabolites controlling tumorigenesis, including excess succinate that is referred to as “oncometabolite” [17]. Using genetically engineered mouse cells, investigators have established that loss of *SDHB* promotes cell proliferation via pyruvate carboxylation, succinate-induced hypoxia-inducible factor alpha (HIF $\alpha$ ) stabilization, and enhanced gene methylation [16,18,19]. Data from these studies has provided valuable insight into the metabolic pathogenesis of PCC/PGL with *SDHx* mutations. Genetic characterization of PCC/PGL [7] provided a unique opportunity for a comprehensive understanding of this rare neuroendocrine tumor by complementing it with metabolomic analysis of the same, extensively documented, tumor sets.

Several studies have indicated that neuroblastomas exhibit closely associated behavior with PCC/PGL, and recent work has shown that the polyamine pathway plays a key role in neuroblastoma pathogenesis. Polyamines (putrescine, spermidine and spermine) are ubiquitous polycations that bind nucleic acids and proteins. They play essential roles in many fundamental processes ensuring normal cell growth, including protein and nucleic acid metabolism, chromatin organization, ion channel control, and cell death regulation. Polyamines are required to maintain cell proliferation. The interplay between overcharged polyamine metabolism and several cancer pathways holds notable promise for drug therapy (reviewed in [20,21]). The data on polyamine pathway in the adrenal medulla is scarce [22,23].

While the role of polyamine pathway has not been previously considered for PCC/PGL, the possible link between neuroblastomas and the polyamine pathway was recognized thirty years ago [24]. Neuroblastoma, together with PCC and PGL, constitute the three known types of primary tumors that arise from the autonomic nervous system [25,26]. Several genetic alterations have been described for neuroblastoma, most prominently amplification of *MYCN* proto-oncogene that predicts poor outcome [27,28]. With respect to polyamine metabolism, ornithine decarboxylase (ODC, encoded by the *ODCI* gene) is the key rate-limiting enzyme in polyamine synthesis pathway that converts ornithine to putrescine; its expression and function are tightly regulated at multiple levels [28]. *ODCI* was one of the first direct *MYC* targets discovered and these genes are frequently co-amplified [29,30]. Importantly, even in the absence of *MYCN* amplification, *ODCI* is overexpressed in high-risk compared to lower-risk tumors, and this overexpression is associated with reduced survival [31-33]. These earlier observations and several recent breakthroughs in understanding the role of the polyamine pathway in neuroblastoma [34,35] suggest that over-active polyamine pathway could be an important negative factor in all primary autonomic nervous system tumors.

Suppressing polyamine synthesis by targeting ODC to curb tumor growth has been previously proposed (reviewed in [36]). Importantly, homeostatic cellular polyamine concentrations are maintained through a finely orchestrated balance of synthesis and degradation as well as uptake and export. Targeting polyamine pathway for therapeutic purposes has to take these multiple processes into consideration. In this respect, down-regulation of ODC activity by its inhibitor difluoromethylornithine (DFMO) triggers compensatory increase in polyamine uptake [37,38]. While the mechanisms of polyamine transport are not entirely understood, synthetic polyamine analogues were developed that resemble natural polyamines, but do not support cellular growth [39]. These compounds could successfully reduce cellular polyamine concentrations while simultaneously jamming their import from the extracellular milieu.

Since succinate dehydrogenase mutations in PCC/PGL are associated with aggressive disease, we hypothesized that a down-regulation in the active succinate dehydrogenase B subunit should result in notable changes in cellular metabolic profile and could present a vulnerability point for successful pharmacological targeting. To examine the importance of the polyamine pathway in PCC/PGLs, we performed metabolite analysis on the progenitor human cell line originated from a PCC, hPheo1 wild-type (WT) [40] and its derivative,

hPheo1 *SDHB* knockdown (KD) cells. We found that the polyamine pathway was up-regulated in hPheo1 *SDHB* KD cells and confirmed these results with PCC/PGL tissue samples with *SDHx* mutations.

## 2. Materials and methods

### 2.1. Cell culture

The hPheo1 WT cell line derived from a human progenitor PCC was previously described [40]. hPheo1 WT cells and hPheo1 *SDHB* KD cells were cultured in RPMI 1640 with 10% FBS. The BJ fibroblast cell line was cultured in DMEM with 10% FBS.

The metabolite extraction protocol was previously described [41] and used here with minor modifications. A six well plate (60 mm dish size) of hPheo1 WT cells and hPheo1 *SDHB* KD cells ( $3 \times 10^6$ ) were grown in RPMI with 10% FBS and used for the extraction of intracellular metabolites after 72 h. Media was aspirated and cells were washed twice with 5% mannitol solution (10 mL first and then 2 mL). 800  $\mu$ L of Optima LC/MS grade methanol (Fisher Scientific, Fairlawn, NJ, USA) was added to cells for 30 s to inactivate enzymes. Next, the cell extract was treated with 550  $\mu$ L of internal standards solution provided by Human Metabolome Technology, Inc., Tsuruoka, Japan (H3304-1002, Human Metabolome Technologies, Inc., Tsuruoka, Japan) and left undisturbed for another 30 s. The extract was obtained and centrifuged  $2300 \times g$  at 4 °C for 5 min. 800  $\mu$ L of upper aqueous layer was centrifugally filtered through a Millipore 5-kDa cutoff filter at  $9100 \times g$  and 4 °C for 5 h to remove proteins. The filtrate was centrifugally concentrated and resuspended in 50  $\mu$ L of Milli-Q water for CE-TOF/MS analysis.

### 2.2. *SDHB* knockdown, transduction and validation

A total of  $2 \times 10^5$  hPheo1 WT cells were seeded in 24 well plates and 750  $\mu$ L of SMARTvector Lentiviral Human *SDHB* shRNA (Dharmacon) were transfected using Polybrene Infection/Transfection Reagent (EMD Millipore, USA) and incubated overnight. Post-24 h, cells were rescued with ACL-4 media containing serum. At 48 h post-transfection, cells were selected via addition of 500  $\mu$ g/mL of puromycin for several weeks. RNA from puromycin-resistant cells was isolated and assayed by qRT-PCR.

### 2.3. Cell line metabolomic analysis

The metabolites were analyzed by using a fused silica capillary (50  $\mu$ m i.d.  $\times$  80 cm total length), with commercial electrophoresis buffer (Solution ID: H3301-1001 for cation analysis (Solution ID: H3301-1001 for cation analysis; Solution ID: H3302-1021 for anion analysis), both from Human Metabolome Technologies) as the electrolyte. The sample was injected at a pressure of 50 mbar for 10s (approximately 10 nL) in cation analysis and 25 s (approximately 25 nL) in anion analysis. The spectrometer was scanned from  $m/z$  50 to 1000. Other conditions were as previously described [42,43].

Peaks were extracted using automatic integration software MasterHands (Keio University, Tsuruoka, Japan) to obtain peak information including  $m/z$  and migration time for CE-TOF/MS measurement (MT), and peak area [44]. Signal peaks corresponding to

isotopomers, adduct ions, and other product ions of known metabolites were excluded, and remaining peaks were annotated with putative metabolites from the HMT metabolite database based on their MTs and  $m/z$  values determined by TOF/MS (Supplemental Table 1). The tolerance range for peak annotation was configured at  $\pm 0.5$  min for MT and  $\pm 10$  ppm for  $m/z$ . In addition, peak areas were normalized against those of internal standards and then the resultant relative area values were further normalized by sample amount using (Eq. (1)).

$$\text{Relative Peak Area} = \frac{\text{Metabolite Peak Area}}{\text{Internal Standard Peak Area} \times \text{Sample Amount}} \quad (1)$$

Metabolome measurements were carried out in a facility service at Human Metabolome Technology Inc. (Tsuruoka, Japan).

## 2.4. Human tissue

**2.4.1. PCC/PGL SDHB-deficient tumor samples**—Fresh frozen PCCs/PGLs were collected under protocols that also allowed for collection of ENSAT registry and biobank protocols as previously described [45]. PCC/PGL tumors were obtained from University Hospital Carl Gustav Carus, Technische Universität Dresden, Germany; NIH, USA; UniversitätsSpital Zurich, Switzerland; Tufts Medical Center, USA; Spanish National Cancer Research Center (CNIO), Spain; Radboud University Medical Center, Netherlands; Aix Marseille Université, France; and University of Würzburg, Germany. Ten normal adrenal medulla tissue specimens were from the University of Alabama, USA. Tumor procurement was approved under Institutional Review Boards from each respective center/institution and it was used for validation of identified metabolites from hPheo1 *SDHB* KD and hPheo1 WT cell lines.

**2.4.2. (A) Human tumor sample preparation**—Adrenal tumor tissue (~5 to 10 mg) was homogenized in 5 mM ammonium acetate at 1800 rpm for 30 s. After 30 min incubation on ice, supernatant was collected by centrifuging at 20,000  $\times$ g for 10 min at 4 °C. This supernatant was normalized to the amount of protein in the samples. Protein concentration was determined using Qubit protein quantification kit (Thermo Fisher, San Jose, CA). Following addition of 10  $\mu$ L of internal standard solution, metabolites were extracted by adding 8:1:1 Acetonitrile: Methanol: Acetone (v/v) and incubating for 30 min at 4 °C. The internal standard solution consisted of D-Leucine-D<sub>10</sub>(C/D/N Isotopes, Pointe-Claire, Quebec, Canada), L-Tryptophan-2,3,3-D<sub>3</sub> (C/D/N Isotopes), Succinic Acid-2,2,3,3-d<sub>4</sub>(C/D/N Isotopes), L-Tyrosine Ring-<sup>13</sup>C<sub>6</sub> (Cambridge Isotope Laboratories, Tewksbury, MA, USA), L-Leucine-<sup>13</sup>C<sub>6</sub> (Cambridge Isotope Laboratories), L-Phenylalanine Ring-<sup>13</sup>C<sub>6</sub> (Cambridge Isotope Laboratories), N-BOC-L-*tert*-Leucine (Acros Organics, Fairlawn, NJ, USA), and N-BOC-L-Aspartic Acid (Acros Organics). Supernatant was dried under a gentle stream of nitrogen at 30 °C. 50  $\mu$ L of reconstitution solution consisted of BOC-L-Tyrosine, BOC-L-Tryptophan and BOC-D-Phenylalanine was added and samples were analyzed by LC-HRMS [46].

## 2.5. Metabolite analysis by LC-HRMS

LC-HRMS metabolite analysis was conducted at the Southeast Center for Integrated Metabolomics (SECIM) at the University of Florida. Analysis was performed on a Thermo Q-Exactive Orbitrap mass spectrometer with Dionex UHPLC and autosampler. Samples were analyzed in positive and negative heated electrospray ionization (mass resolution of 35,000 at  $m/z$  200) using separate injections (volumes of 2  $\mu$ L for positive and 4  $\mu$ L for negative were injected). Separation was achieved on an ACE 18-PFP 100  $\times$  2.1 mm, 2  $\mu$ m column with 0.1% formic acid in water as mobile phase A and acetonitrile as mobile phase B. Flow rate was maintained at 350  $\mu$ L/min with a column temperature of 25  $^{\circ}$ C [46]. An internally curated metabolite library of 1100 compounds was used for metabolite identification by matching retention time ( $\pm$  0.2 min) and  $m/z$  value (5 ppm for positive and 10 ppm for negative). Metabolites of 115 fresh frozen samples (31 human PCC/PGL tumor samples carrying *SDHx* mutations, 74 non-*SDHx* mutated tumor samples, along with 10 normal adrenal medullae as controls) were profiled (Supplemental Table 2). Metabolite descriptions and pathways were derived using the Kyoto Encyclopedia of Genes and Genomes (KEGG) Database and the Human Metabolome Database (HMDB).

## 2.6. Tumor data

Analysis of raw tumor metabolite data was performed on El-Maven as previously described (<https://doi.org/10.5281/zenodo.2537593>) [47]. Thermo.raw format files were converted to an open source format (mzML) using the msConvert tool from ProteoWizard [48]. Compound database used for processing was derived from KEGG database, with final compound database inclusive of all the compounds found in all of the KEGG's reaction databases. Automated peak picking feature of El-Maven was then used to get the peak intensity of all the metabolites. Polyamine metabolites were observed in positive mode. Cyclic Loess normalization [49] was performed followed by normalization with internal and injection standards to correct for any sample preparation biases or analytical errors. Batch effect correction was performed using edgeR package in R to correct for batch differences [50]. Differential expression analysis was performed using limma package in R to identify metabolites differentially enriched in different cohorts of interest [51].

## 2.7. Network analysis

Network analysis was performed on Polly IntOmics [52]. Polly IntOmics is an integrated omics analysis tool based on GAM [53] and used to generate pathway level insights from metabolomics data. The network map was generated through Cytoscape and Inkscape tools [54]. See Supplemental Fig. 1 for Cytoscape analysis.

## 2.8. In-vitro drug testing by clonogenic assay

To measure the  $IC_{50}$  of polyamine inhibitors, 500 hPheo1 WT cells and hPheo1 *SDHB* KD cells were plated per well in six well plates. After 24 h, these plates were treated with DENSPM and DESPM concentrations between 10 and 75 nM for 10 days [55]. Human BJ fibroblast cells were used as controls in colony forming assays.

After 10 days, the cells were stained with filter sterilized Crystal Violet (0.1%, 25 mL methanol cell culture grade, 75 mL sterilized water) solution, 1.0 mL/well for 30 min. Plates

were washed with distilled water and air dried overnight at room temperature. Then, they were scanned and colony frequency was measured and normalized with Image J (NIH, Bethesda, MD, USA) software version 1.4.

## 2.9. Spheroid protocol for injections

Cells were seeded at  $5 \times 10^4$ /mL in 7 mL of DMEM/F12 medium containing 2% B27, 1% penicillin/streptomycin, EGF (20 ng/mL) and bFGF (10 ng/mL) in ultra-low attachment T25 flasks (Corning). After a week, cells were passaged into 15 mL of the medium at a density of  $5 \times 10^4$ /mL into T75 ultra-low flask and incubated for another week. Cell strainer was used to eliminate single cells. Cell clusters were washed with the collected medium, and the clusters were spun down at  $900 \times g$  for 10 min at 4 °C.  $1.5 \times 10^6$  accutase (ThermoFisher) was added to the cell pellet and incubated for 10–30 min at 37 °C in CO<sub>2</sub> incubator. Cells were gently pipetted during the incubation several times. After dissociation, cells were spun down and re-suspended in DMEM/F12 medium. Cells were counted and  $7.5 \times 10^5$  cells/mouse injection were seeded and incubated for a week. The cell suspension containing spheres was transferred into a 50 mL tube and spun down at  $900 \times g$  for 10 min. Supernatant was discarded and the sphere pellet re-suspended in PBS, 100  $\mu$ L/mouse injection. Spheroids were kept on ice until the injection.

## 2.10. Animals

Commercial athymic scid male mice (Taconic C-B-Igh-1b/IcrTac-Prkdcscid) were used to generate a xenograft model of PCC/PGL. Animals were obtained from the vendor at 5 weeks and allowed to acclimate for two additional weeks. Subcutaneous tumors using hPheo1 WT and hPheo1-*SDHB* KD cells were created as previously described [56,57].  $2 \times 10^6$  cells grown as spheroids were re-suspended in PBS and injected subcutaneously into the right flank of animals. The control cohort was injected with PBS only. Animals were monitored biweekly until tumors started to appear (were palpable) at approximately two months, at which point animals were monitored daily. When the tumors reached a well-defined, caliper-measurable size (100–200 mm<sup>3</sup>), animals carrying either hPheo1 WT or hPheo1 *SDHB* KD xenografts were inspected by the MRI and divided into two groups, the PBS-injected (control group) or DENSPM-injected (treated group). The protocol to examine the effects of DENSPM in xenograft animals was approved by the UF IACUC (Study #201609547). Once the tumor in the untreated animals reached the predetermined size of ~2000 mm<sup>3</sup>, they were inspected by the MRI, sacrificed and tumor tissue preserved. Furthermore, MRI was used to detect tumors and measure tumor growth by volumetric assessment at the completion of the experiment. Between MRI procedures, tumors were measured every other day using digital caliper and tumor volume (V) was calculated using the formula  $V = ab^2 \times 0.52$ , where a and b are major and minor axes of the tumor foci, respectively. hPheo1 WT and hPheo1-*SDHB* KD-injected mice with tumor volume at ~100 mm<sup>3</sup> were divided into two following treatment groups with similar tumor volume distribution: (1) vehicle or (2) DENSPM administered by intraperitoneal injection at 60 mg/kg QD. The concentration of the DENSPM was based on previous work [58]. Bernacki et al. [58] observed some toxicity and weight loss at a dose of 80 mg/kg so here a lower dose (60 mg/kg) and lower frequency of administration (QD vs. TID) was used. All treated animals were kept on treatment for 46 days, at which point they were inspected by the MRI,

sacrificed and tumor tissue (if any) preserved. Animal weight and normal activity were monitored.

### 2.11. MRI procedures

Mice were imaged using a MR Solutions quadrature birdcage in a mouse cradle (Minerve Equipement Veterinaire, Esternay, France) maintained at 37 °C. Hearing protection and eye lubricant were applied and the animals anesthetized with 2% to 2.5% isoflurane at 0.8 L/min oxygen flow rate. Respiration was monitored (SA Instruments Inc., Stony Brook, NY) using a respiration pillow sensor under the abdomen. Waste gas and CO<sub>2</sub> were actively scavenged. Total scan time including localizer acquisitions was 30–45 min during which anesthesia level was adjusted to maintain a respiration rate of 40–50 breaths/min. In vivo high-resolution MRI data was collected on a 7 T MRI system (MR Solutions Ltd., Guildford, UK) equipped with a shielded gradient system with 300-mT/m gradient strength and a clear-bore diameter of 90 mm. Scout localizer images were collected with a gradient-echo sequence followed by T1-weighted anatomical images (RARE; TE = 8 ms) to confirm the slice package. This slice package was used to collect T2-weighted data for analysis. Twenty-four contiguous slices 1 mm thick were collected using RARE with standard CHES Fat Suppression. Field of view was 32 mm × 32 mm and the matrix size was 400 × 256 which provided an in-plane resolution of 80 μm × 125 μm. Initial TE was 70 ms and the echo train length was 8 with echo spacing of 10 ms. TR was 4 s and the number of acquisitions was equal to 4 resulting in a total acquisition time of 13.5 min. Mean tumor volumes were measured by drawing regions of interest (ROI), to circumscribe the entire tumor.

### 2.12. Necropsy analysis

Prior to necropsy, the investigator was unaware of the results of the caliper measurements or imaging scans (that were done by different lab personnel), rendering the two analyses independent. 24 h after the last dose (or when the untreated tumors reach >2000 mm<sup>3</sup>), animals were imaged by the MRI and euthanized. Mice were examined at the injection site, tumors excised and weighted. Tumor weights at this point were used as the endpoint reading. To measure the differences between the two tumor models and to gauge DENSPM treatment efficacy, at least 6 animals for each group were measured with calipers on continuous days to obtain longitudinal data and the results were plotted.

### 2.13. Total RNA isolation and quantitative real time (qRT)-PCR

Total RNA were extracted from hPheo1 WT, and hPheo1 *SDHB* KD cells and by the Direct-Zol RNA Miniprep plus Kit (Zymo Research, USA) following the manufacturer's protocol. 20.0 ng of purified RNA were used for Quantitative real-time PCR using Luna® Universal Probe One-Step RT-qPCR Kit (NEB) and Step One Plus Real-time PCR system (Applied Biosystems) following the manufacturer's protocol. GAPDH was a reference gene. Reactions were performed in triplicate using oligonucleotides listed in Supplemental Table 3. *SDHB* gene expression levels were normalized to GAPDH and relative expression was calculated using the comparative threshold cycle method ( $C_T$ ) with the Stepone software (Applied Biosystems). Fold changes in gene expression were calculated with normalized value and represented in Log<sub>2</sub> value on Y-axis.

## 2.14. Western blot

Cells were lysed in 100  $\mu$ L of Pierce IP Lysis buffer with 1 $\times$  final concentration of protease inhibitor (Product: 78430, ThermoFisher Scientific USA), 200 mM EDTA and phosphatase inhibitor (Product: 78428, ThermoFisher Scientific USA) cocktail mixture solution for 30 min on ice and centrifuge at 14000  $\times g$  for 15 min. Clear supernatant was collected in fresh tube and stored at  $-80^{\circ}\text{C}$  until further use. 60  $\mu$ g of whole cell protein extract of hPheo1 WT and hPheo1 *SDHB* KD were separated by 4–20% sodium dodecyl sulfate polyacrylamide gel electrophoresis and transferred to PVDF membrane (Millipore, Bedford, MA). After blocking with 5% dry milk in 1 $\times$  TBST (Tris base pH 7.4, KCl 2.7 mM, NaCl 137 mM and 0.01% Tween) for 2 h at room temperature, membranes were incubated with the primary antibodies against SDHB (1:2000), and eEF2 (1:2000) in dilution buffer overnight at  $4^{\circ}\text{C}$ . Membranes were washed for three times with TBST and incubated with HRP conjugated mouse secondary antibody (NA931-1ML) and Rabbit IgG, HRP-linked Whole Ab (NA934-1ML) with 1:5000 dilution. PVDF blots were developed using hyBlot CL (Denville Scientific, Inc., USA) autoradiography film. Signal was normalized with eEF2 internal loading control and fold difference was measured by Image J software (NIH, Bethesda, USA).

Antibodies used were as follows: SDHB (Ab14714, Abcam) and eEF2 (#2332, Cell Signaling Technology), and Rabbit IgG, HRP-linked Whole Ab (NA934-1ML), HRP conjugated mouse secondary antibody (NA931-1ML) (Thermo Fisher Scientific, Waltham, MA).

## 2.15. Statistical analysis

Data are expressed as mean  $\pm$  SE. Comparisons between groups were determined using Student's *t*-test for normally-distributed variables and Kruskal-Wallis for non-parametric variables. Due to small sample size, cell line-based analyses were also performed with non-parametric tests. *p* values of  $<0.05$  were considered statistically significant. Statistical analyses were performed with Stata 11.1 (StataCorp LP, College Station, TX) and Prism 6.0 (GraphPad Software, Inc., La Jolla, CA).

## 3. Results

### 3.1. hPheo1 *SDHB* KD cells

hPheo1 *SDHB* KD cells were generated as described in the Materials and Methods section and *SDHB* expression was analyzed. Delta Ct value was normalized with *GAPDH* and data represented in  $\text{Log}_2$  value on Y-axis (Fig. 1A). The qRT-PCR shows a decrease in *SDHB* mRNA expression in hPheo1 *SDHB* KD compared to hPheo1 WT (Fig. 1A). Since *SDHB* RNA is reduced but not absent in hPheo1 cells, hPheo1 WT and hPheo1 *SDHB* KD cells were examined for the presence of SDHB protein expression using immunoblot (Fig. 1B); ubiquitous (e.g., [59]) eukaryotic translation elongation factor 2, eEF2 was used as a loading control as it tracks well in these cells with other customarily used loading controls. As shown in Fig. 1, hPheo1 *SDHB* KD showed significantly reduced levels of mRNA, and almost complete absence of SDHB protein expression (4).

### 3.2. Polyamine metabolism

To assess the metabolic changes in hPheo1 cell line after *SDHB* KD, succinate levels were measured, which were significantly higher in hPheo1 *SDHB* KD cells compared to hPheo1 WT cells (Fig. 2). Analysis of 31 primary tumor samples with *SDHx* mutations demonstrated a 20-fold increase in succinate levels compared to non-*SDHx*-mutated adrenal tumor samples ( $p < .001$ ) (Fig. 2), in line with previously reported data [60].

Specifically evaluating the polyamine pathway, we discovered it to be significantly over-activated in hPheo1 *SDHB* KD cells compared to WT cells. In order to confirm this data, we used *SDHx* mutated tumor tissue (*SDHAF2* [ $n = 1$ ], *SDHB* [ $n = 18$ ], *SDHC* [ $n = 3$ ], and *SDHD* [ $n = 9$ ]) compared to non-*SDHx* mutated tumor samples. Particularly, significant increases for spermidine and spermine (Fig. 2) were observed in human *SDHx* mutated PCC/PGLs, with a similar pattern in hPheo1 *SDHB* KD cells, although spermidine did not reach statistical significance in cell line experiments. On the other hand, putrescine (Fig. 2) showed decreased levels in hPheo1 *SDHB* KD cells, but not in human *SDHx*-mutated samples. Of note, in a sub-analysis comparing only *SDHB* metastatic samples ( $n = 6$ ) to normal adrenal medulla ( $n = 10$ ), we observed an overall similar trend. Both spermidine and spermine were higher in metastatic samples with *SDHB* mutation, although they did not reach statistical significance. However, ornithine and putrescine, which are upstream of spermidine and spermine in the polyamine pathway, did reach statistical significance when *SDHB* malignant samples were compared to normal adrenal medulla ( $2.8 \pm 0.6$  vs.  $1.0 \pm 0.3$ ,  $p = .008$ ;  $2.1 \pm 0.4$  vs.  $1.0 \pm 0.2$ ,  $p = .012$ , respectively). Also, when comparing metastatic *SDHB* samples ( $n = 6$ ) versus benign *SDHB* samples ( $n = 12$ ) ornithine levels were statistically higher in metastatic samples compared with benign samples ( $2.8 \pm 0.6$  vs.  $1.6 \pm 0.2$ ,  $p = .023$ , respectively). In terms of functional tumors, evaluating *SDHx* tumors making dopamine/norpephrine ( $n = 93$ ) compared to *SDHx* tumors that were nonfunctional ( $n = 8$ ), *SDHx* functional samples had significantly lower putrescine ( $1.5 \pm 0.1$  vs.  $2.7 \pm 0.7$ ,  $p = .009$ ) and spermidine ( $4.0 \pm 1.3$  vs.  $15.7 \pm 5.3$ ,  $p = .003$ ). When specifically comparing *SDHB* functional vs. *SDHB* non-functional samples, a trend towards lower putrescine ( $1.6 \pm 0.2$  vs.  $3.1 \pm 2.0$ ,  $p = .07$ ) and spermidine ( $2.7 \pm 1.1$  vs.  $11.5 \pm 10.8$ ,  $p = .06$ ) in functional *SDHB* was observed (Fig. 2).

Overall, these results are consistent with polyamine pathway overactivity with increased production of spermidine and spermine, which is more significant in non-functional (i.e., less differentiated) tumor samples. While this is enough to produce a significant reduction of putrescine levels in hPheo1 *SDHB* KD cells, it is likely that sustained influx of substrate in human adrenal tumors is able to maintain the increased polyamine pathway activity without causing putrescine depletion.

### 3.3. Colony formation assay with polyamine analogs

Differences in levels of polyamine pathway components in hPheo1 WT and hPheo1 *SDHB* KD cell lines prompted us to examine their response to polyamine analogue inhibitor (DENSPM and DESPM) treatment. All three cell lines (BJ fibroblasts, hPheo1 WT and hPheo1 *SDHB* KD) demonstrated different doubling times. BJ fibroblasts, hPheo1 WT, and hPheo1 *SDHB* KD cells were cultured and treated with different doses of DENSPM ranging

between 10 nM–75 nM with 500 cells/well (Fig. 3A). DENSPM dose response curves showed IC<sub>50</sub> value for hPheo1WT at 75 nM whereas hPheo1 *SDHB* KD showed a response at 40 nM (Fig. 3B). On the other hand, BJ fibroblasts showed no sensitivity towards DENSPM at this concentration range (Fig. 3B). For DESPM, the dose response data demonstrated a very low IC<sub>50</sub> for hPheo1 *SDHB* KD at 10 nM, whereas hPheo1 WT showed an IC<sub>50</sub> of 50 nM (Fig. 3C and D).

### 3.4. Animal xenograft experiments

The remarkable growth suppression of hPheo1 cell growth by DENSPM and DESPM encouraged us to investigate in vivo effect of polyamine inhibitors. DENSPM was chosen for in vivo studies due to its reported lower toxicity [61]. The antitumor effect of DENSPM was evaluated in the xenograft model as described in the Methods. No significant weight loss or signs of toxicity (i.e., diarrhea, abdominal stiffness, lethargy) were noted at that concentration in the treated group (60 mg/kg DENSPM by intraperitoneal injection) compared to vehicle. Tumor size was measured with digital calipers and tumor volume was calculated (Fig. 4A). DENSPM administration resulted in a reduction of tumor volume, with tumor growth inhibition (TGI) reaching 75% and 86% in hPheo1 and hPheo1 *SDHB* KD cohorts, respectively. DENSPM significantly reduced tumor volume relative to control between days 16 and 36, with a TGI of ~66% in both cohorts by day 16. Tumor weight in treated animals was also significantly reduced compared to vehicle-injected mice (Fig. 4B). Quantitative assessment of tumor growth was additionally performed by MRI (Fig. 4C). MRI confirmed DENSPM-mediated tumor regression (i.e., tumor being smaller by the end of the experiment) in 8 out of 10 hPheo1 *SDHB* KD mice with an overall 87% regression in tumor volume relative to the first MRI measurement (3 days after the beginning of treatment).

## 4. Discussion

In order to identify new altered metabolic pathways due to *SDHx* mutations, we conducted a metabolite analysis in hPheo1 WT and hPheo1 *SDHB* KD cells and confirmed our results in human PCC/PGLs tissue since there is only one progenitor human cell line derived from PCC in existence. As shown in Fig. 2 of the present study, with *SDHB* KD in hPheo1 cells, there was an elevation in succinate compared to hPheo1WT. Moreover, this finding was further confirmed in experiments performed in human tumor tissue. These results are in accordance with prior reports [60,62-65] suggesting that *SDHx* mutations lead to the accumulation of succinate, which in turn can act as oncometabolite, altering gene expression and epigenetic regulation and favoring PCC/PGL progression [17,66].

Moreover, hPheo1 *SDHB* KD cells also showed increased polyamine pathway end products (i.e., spermidine and spermine), suggesting that this pathway may be up-regulated in these tumors. This trend was confirmed in PCC/PGL *SDHx* human tumors. Furthermore, polyamine substrate increases appeared to be more significant among non-functional tumors, suggesting that upregulation of this pathway may play a role in the survival of more undifferentiated tumors. These findings were consistent among all *SDHx* mutated samples, but also when the analyses were limited to *SDHB* samples. The reasons for the elevation of

the polyamines in cells with altered TCA cycle metabolism is currently under investigation. It has been demonstrated that in the adrenal gland, the polyamine, putrescine (and not glutamic acid), serves as a sole precursor for gamma-aminobutyric acid (GABA) synthesis [67]. Under certain circumstances, GABA can be converted to succinate and enter the tricarboxylic acid cycle (TCA), through the so-called “GABA shunt” pathway [68]. It is possible that excess succinate leads to the feedback inhibition of GABA synthesis and accumulation of polyamine products.

Recent advances highlighted the importance of the polyamine pathway in a type of tumor closely related to PCC/PGL, such as neuroblastoma. It was long known that autonomic nervous system tumors have many important features in common, and similar features between PCC/PGL and neuroblastoma have been reported (e.g., [69-71]). Recent research highlighted the role for solute carrier family 3 member 2 (SLC3A2) as an essential transporter necessary for polyamine uptake in neuroblastoma [34]. The uptake of radiolabeled spermidine was reduced in cells with knockdown of SLC3A2 in neuroblastoma cells. Furthermore, inhibition of polyamine uptake combined with the suppression of the polyamine synthesis through ODC1 inhibition abrogated tumor development in neuroblastoma-prone mice [34]. Therefore, we hypothesized that as polyamine pathway appears to be up-regulated in hPheo1 *SDHB* KD cells, they would be sensitive to chemically synthesized polyamine pathway inhibitors *N*<sup>1</sup>,*N*<sup>11</sup>-diethylnorspermine (DENSPM) and *N*<sup>1</sup>,*N*<sup>12</sup>-diethylspermine (DESPM) even at low concentrations, ranging from 10 nM–100 nM (see Fig. 3). When the cell lines were treated with DESPM, hPheo1 *SDHB* KD cells were found to be more sensitive compared to hPheo1 WT. However, both hPheo1 cell lines were more sensitive to DENSPM compared to human fibroblasts. Although a more dramatic effect was seen with DESPM treatment of hPheo1 *SDHB* KD cells compared to hPheo1 WT, we used DENSPM for in vivo experiments as DENSPM is currently being examined in human clinical trials in other cancers as it is less toxic than DESPM [55]. This is consistent with the observations of a number of different cancer tumor lines [55,61].

Based on these findings, we tested polyamine pathway inhibitors to examine their effect on cellular proliferation in vitro and in mouse xenograft models. We also showed here that DENSPM significantly decreases tumor growth in vivo in our physiologically relevant, patient-derived cell line xenograft mouse model. Taken together, these results suggest that delivery of a well-tolerated dose of DENSPM will result in substantial activity against PCC/PGL derived tumors. Better understanding of the mechanistic basis of action for polyamine analogue compounds in PCC/PGL will inform a new therapeutic approach for patients with metastatic disease.

## 5. Conclusion

Novel to the understanding of PCC/PGL pathophysiology is that there is a significant up-regulation of the polyamine pathway in hPheo1 *SDHB* KD cells as well as in human *SDHB* tumor tissues. Furthermore, treatment with polyamine inhibitors significantly inhibited hPheo1 cell growth and led to growth inhibition in xenograft mice treated with DENSPM (Fig. 5). These results provide new foundation for exploring the role for polyamine analogue

inhibitors in treating metastatic PCC/PGL. However, further translational research studies are needed to explore if this drug can be considered for clinical use in PCC/PGL patients.

## Supplementary Material

Refer to Web version on PubMed Central for supplementary material.

## Acknowledgements

The authors would like to thank the patients, their families, and the administration of SDHB PheoParaCoalition for supporting this research. This work was also supported by the Gatorade Trust through funds distributed by the University of Florida, Department of Medicine, and Pilot Funding Initiative of the North Florida/South Georgia (NF/SG) VA HS Research Service to HKG.

### Funding

This research was supported by the Gatorade Trust Fund from the Department of Medicine, University of Florida Gatorade (Project# 00122235), Southeast Center for Integrated Metabolomics- University of Florida, SDHB PheoPara Coalition, and Malcom Randall VA Pilot Award Program (H.K.G); *Eunice Kennedy Shriver* National Institute of Child Health and Human Development, National Institutes of Health (K.P.). The sponsors had no involvement in study design, in the collection, analysis and interpretation of data. in the writing of the report and in the decision to submit the article for publication.

## References

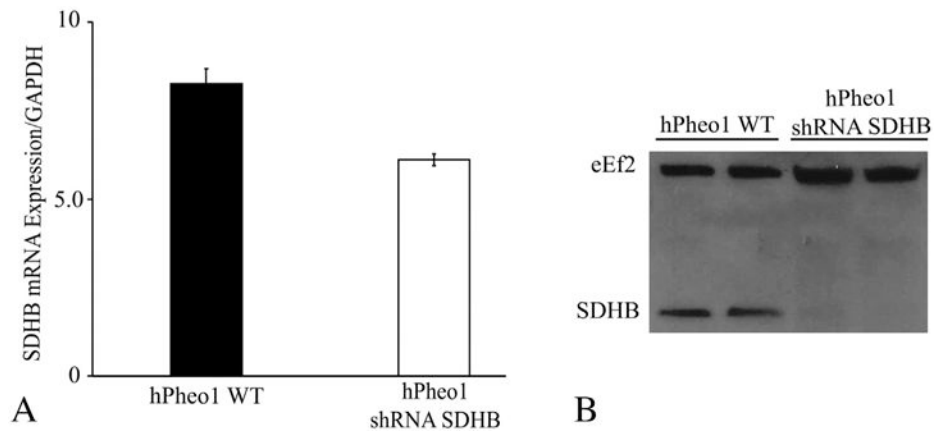
- [1]. Ziegler RG, Weinstein SJ, Fears TR. Nutritional and genetic inefficiencies in one-carbon metabolism and cervical cancer risk. *J Nutr.* 2002;132:2345S–9S. 10.1093/jn/132.8.2345S. [PubMed: 12163690]
- [2]. Turkova H, Prodanov T, Maly M, Martucci V, Adams K, Widimsky J Jr, et al. Characteristics and outcomes of metastatic Sdhb and sporadic pheochromocytoma/paraganglioma: an National Institutes of Health study. *Endocr Pract.* 2016;22:302–14. 10.4158/EP15725.OR. [PubMed: 26523625]
- [3]. Hamidi O Metastatic pheochromocytoma and paraganglioma: recent advances in prognosis and management. *Curr Opin Endocrinol Diabetes Obes.* 2019;26:146–54. 10.1097/MED.0000000000000476. [PubMed: 30893083]
- [4]. Lenders JW, Eisenhofer G, Mannelli M, Pacak K. Pheochromocytoma. *Lancet.* 2005;366:665–75. 10.1016/S0140-6736(05)67139-5. [PubMed: 16112304]
- [5]. Nolting S, Grossman A, Pacak K. Metastatic Pheochromocytoma: spinning towards more promising treatment options. *Exp Clin Endocrinol Diabetes.* 2018;127:117–28. <https://doi.org/m1055/a-0715-1888>. [PubMed: 30235495]
- [6]. Baudin E, Habra MA, Deschamps F, Cote G, Dumont F, Cabanillas M, et al. Therapy of endocrine disease: treatment of malignant pheochromocytoma and paraganglioma. *Eur J Endocrinol.* 2014;171:R111–22. 10.1530/EJE-14-0113. [PubMed: 24891137]
- [7]. Fishbein L, Leshchiner I, Walter V, Danilova L, Robertson AG, Johnson AR, et al. Comprehensive molecular characterization of pheochromocytoma and paraganglioma. *Cancer Cell.* 2017;31:181–93. 10.1016/j.ccell.2017.01.001. [PubMed: 28162975]
- [8]. Dahia PL, Ross KN, Wright ME, Hayashida CY, Santagata S, Barontini M, et al. A HIF1alpha regulatory loop links hypoxia and mitochondrial signals in pheochromocytomas. *PLoS Genet.* 2005;1:72–80. 10.1371/journal.pgen.0010008. [PubMed: 16103922]
- [9]. Burnichon N, Vescovo L, Amar L, Libe R, de Reynies A, Venisse A, et al. Integrative genomic analysis reveals somatic mutations in pheochromocytoma and paraganglioma. *Hum Mol Genet.* 2011;20:3974–85. 10.1093/hmg/ddr324. [PubMed: 21784903]
- [10]. Lussey-Lepoutre C, Buffet A, Gimenez-Roqueplo AP, Favier J. Mitochondrial deficiencies in the predisposition to Paraganglioma. *Metabolites.* 2017;7 10.3390/metabo7020017.

- [11]. Gimenez-Roqueplo AP, Dahia PL, Robledo M. An update on the genetics of paraganglioma, pheochromocytoma, and associated hereditary syndromes. *Horm Metab Res.* 2012;44:328–33. 10.1055/s-0031-1301302. [PubMed: 22328163]
- [12]. Crona J, Lamarca A, Ghosal S, Welin S, Skogseid B, Pacak K. Genotype-phenotype correlations in pheochromocytoma and paraganglioma. *Endocr Relat Cancer.* 2019 10.1530/ERC-19-0024.
- [13]. Amar L, Bertherat J, Baudin E, Ajzenberg C, Bressac-de Paillerets B, Chabre O, et al. Genetic testing in pheochromocytoma or functional paraganglioma. *J Clin Oncol.* 2005;23:8812–8. 10.1200/JCO.2005.03.1484. [PubMed: 16314641]
- [14]. Benn DE, Gimenez-Roqueplo AP, Reilly JR, Bertherat J, Burgess J, Byth K, et al. Clinical presentation and penetrance of pheochromocytoma/paraganglioma syndromes. *J Clin Endocrinol Metab.* 2006;91:827–36. 10.1210/jc.2005-1862. [PubMed: 16317055]
- [15]. Letouze E, Martinelli C, Lorient C, Burnichon N, Abermil N, Ottolenghi C, et al. SDH mutations establish a hypermethylator phenotype in Paraganglioma. *Cancer Cell.* 2013;23:739–52. 10.1016/j.ccr.2013.04.018. [PubMed: 23707781]
- [16]. Cardaci S, Zheng L, MacKay G, van den Broek NJ, MacKenzie ED, Nixon C, et al. Pyruvate carboxylation enables growth of SDH-deficient cells by supporting aspartate biosynthesis. *Nat Cell Biol.* 2015;17:1317–26. 10.1038/ncb3233. [PubMed: 26302408]
- [17]. Sulkowski PL, Sundaram RK, Oeck S, Corso CD, Liu Y, Noorbakhsh S, et al. Krebscycle-deficient hereditary cancer syndromes are defined by defects in homologous-recombination DNA repair. *Nat Genet.* 2018;50:1086–92. 10.1038/s41588-018-0170-4. [PubMed: 30013182]
- [18]. Birsoy K, Wang T, Chen WW, Freinkman E, Abu-Remaileh M, Sabatini DM. An essential role of the mitochondrial electron transport chain in cell proliferation is to enable aspartate synthesis. *Cell.* 2015;162:540–51. 10.1016/j.cell.2015.07.016. [PubMed: 26232224]
- [19]. Lussey-Lepoutre C, Hollinshead KER, Ludwig C, Menara M, Morin A, Castro-Vega LJ, et al. Loss of succinate dehydrogenase activity results in dependency on pyruvate carboxylation for cellular anabolism. *Nat Commun.* 2015;6 10.1038/ncomms9784 ARTN 8784.
- [20]. Casero RA Jr, Murray Stewart T, Pegg AE. Polyamine metabolism and cancer: treatments, challenges and opportunities. *Nat Rev Cancer.* 2018;18:681–95. 10.1038/s41568-018-0050-3. [PubMed: 30181570]
- [21]. Damiani E, Wallace HM. Polyamines and cancer. *Methods Mol Biol.* 1694;2018:469–88. 10.1007/978-14939-7398-9\_39.
- [22]. Ekker M, Sourkes TL. Developmental pattern of ornithine decarboxylase activity, S-adenosylmethionine decarboxylase, and polyamines of rat adrenal glands. *Biol Neonate.* 1987;51:260–7. 10.1159/000242662. [PubMed: 3593807]
- [23]. Schipper RG, Romain N, Otten AA, Tan J, Lange WP, Verhofstad AA. Immunocytochemical detection of ornithine decarboxylase. *J Histochem Cytochem.* 1999;47:1395–404. 10.1177/002215549904701106. [PubMed: 10544213]
- [24]. Tonin PN, Yeger H, Stallings RL, Srinivasan PR, Lewis WH. Amplification of N-myc and ornithine decarboxylase genes in human neuroblastoma and hydroxyurea-resistant hamster cell lines. *Oncogene.* 1989;4:1117–21. [PubMed: 2780050]
- [25]. Maris JM, Hogarty MD, Bagatell R, Cohn SL. Neuroblastoma. *Lancet.* 2007;369:2106–20. 10.1016/S0140-6736(07)60983-0. [PubMed: 17586306]
- [26]. Simo M, Navarro X, Yuste VJ, Bruna J. Autonomic nervous system and cancer. *Clin Auton Res.* 2018;28:301–14. 10.1007/s10286-018-0523-1. [PubMed: 29594605]
- [27]. Brodeur GM, Seeger RC, Schwab M, Varmus HE, Bishop JM. Amplification of N-myc in untreated human neuroblastomas correlates with advanced disease stage. *Science.* 1984;224:1121–4. 10.1126/science.6719137. [PubMed: 6719137]
- [28]. Bachmann AS, Geerts D. Polyamine synthesis as a target of MYC oncogenes. *J Biol Chem.* 2018;293:18757–69. 10.1074/jbc.TM118.003336. [PubMed: 30404920]
- [29]. Bello-Fernandez C, Packham G, Cleveland JL. The ornithine decarboxylase gene is a transcriptional target of c-Myc. *Proc Natl Acad Sci U S A.* 1993;90:7804–8. 10.1073/pnas.90.16.7804. [PubMed: 8356088]

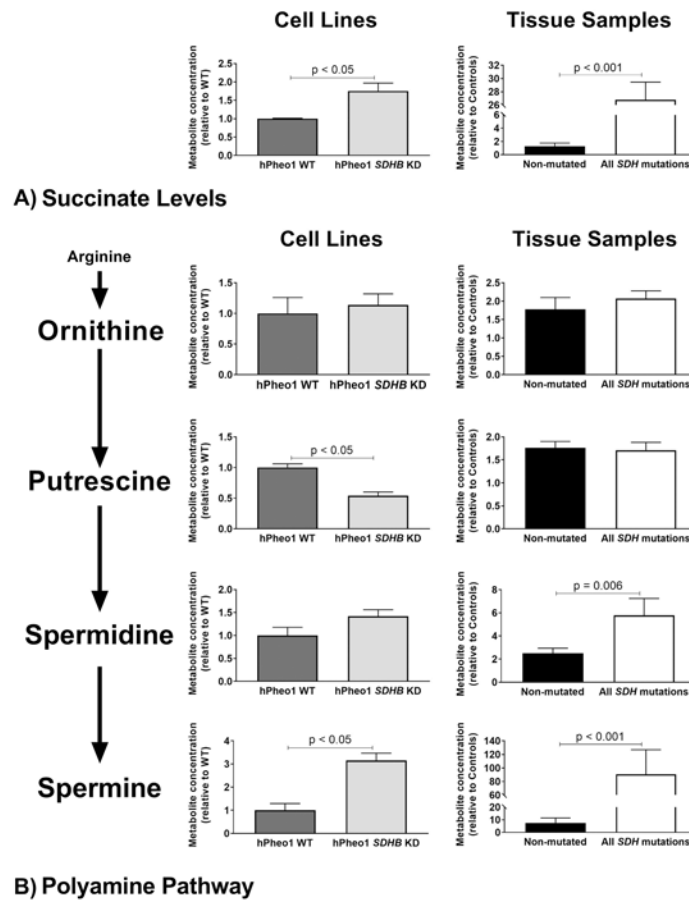
- [30]. Hogarty MD, Norris MD, Davis K, Liu X, Evageliou NF, Hayes CS, et al. ODC1 is a critical determinant of MYCN oncogenesis and a therapeutic target in neuroblastoma. *Cancer Res.* 2008;68:9735–45. 10.1158/0008-5472.CAN-07-6866. [PubMed: 19047152]
- [31]. Geerts D, Koster J, Albert D, Koomoa DL, Feith DJ, Pegg AE, et al. The polyamine metabolism genes ornithine decarboxylase and antizyme 2 predict aggressive behavior in neuroblastomas with and without MYCN amplification. *Int J Cancer.* 2010;126:2012–24. 10.1002/ijc.25074. [PubMed: 19960435]
- [32]. Rounbehler RJ, Li W, Hall MA, Yang C, Fallahi M, Cleveland JL. Targeting ornithine decarboxylase impairs development of MYCN-amplified neuroblastoma. *Cancer Res.* 2009;69:547–53. 10.1158/0008-5472.CAN-08-2968. [PubMed: 19147568]
- [33]. Valentijn LJ, Koster J, Haneveld F, Aissa RA, van Sluis P, Broekmans ME, et al. Functional MYCN signature predicts outcome of neuroblastoma irrespective of MYCN amplification. *Proc Natl Acad Sci U S A.* 2012;109:19190–5. 10.1073/pnas.1208215109. [PubMed: 23091029]
- [34]. Gamble LD, Purgato S, Murray J, Xiao L, Yu DMT, Hanssen KM, et al. Inhibition of polyamine synthesis and uptake reduces tumor progression and prolongs survival in mouse models of neuroblastoma. *Sci Transl Med.* 2019;11 10.1126/scitranslmed.aau1099.
- [35]. Evageliou NF, Haber M, Vu A, Laetsch TW, Murray J, Gamble LD, et al. Polyamine antagonist therapies inhibit neuroblastoma initiation and progression. *Clin Cancer Res.* 2016;22:4391–404. 10.1158/1078-0432.CCR-15-2539. [PubMed: 27012811]
- [36]. Evageliou NF, Hogarty MD. Disrupting polyamine homeostasis as a therapeutic strategy for neuroblastoma. *Clin Cancer Res.* 2009;15:5956–61. 10.1158/1078-0432.CCR-08-3213. [PubMed: 19789308]
- [37]. Sarhan S, Knodgen B, Seiler N. Polyamine deprivation, malnutrition and tumor growth. *Anticancer Res.* 1992;12:457–66. [PubMed: 1580563]
- [38]. Aziz SM, Gillespie MN, Crooks PA, Tofiq SF, Tsuboi CP, Olson JW, et al. The potential of a novel polyamine transport inhibitor in cancer chemotherapy. *J Pharmacol Exp Ther.* 1996;278:185–92. [PubMed: 8764350]
- [39]. Porter CW, Cavanaugh PF Jr, Stolowich N, Ganis B, Kelly E, Bergeron RJ. Biological properties of N4- and N1,N8-spermidine derivatives in cultured L1210 leukemia cells. *Cancer Res.* 1985;45:2050–7. [PubMed: 3921235]
- [40]. Ghayee HK, Bhagwandin VJ, Stastny V, Click A, Ding LH, Mizrahi D, et al. Progenitor cell line (hPheo1) derived from a human pheochromocytoma tumor. *PLoS One.* 2013;8:e65624 10.1371/journal.pone.0065624. [PubMed: 23785438]
- [41]. Lorenz MA, Burant CF, Kennedy RT. Reducing time and increasing sensitivity in sample preparation for adherent mammalian cell metabolomics. *Anal Chem.* 2011;83:3406–14. 10.1021/ac103313x. [PubMed: 21456517]
- [42]. Soga T, Heiger DN. Amino acid analysis by capillary electrophoresis electrospray ionization mass spectrometry. *Anal Chem.* 2000;72:1236–41. [PubMed: 10740865]
- [43]. Soga T, Ohashi Y, Ueno Y, Naraoka H, Tomita M, Nishioka T. Quantitative metabolome analysis using capillary electrophoresis mass spectrometry. *J Proteome Res.* 2003;2:488–94. 10.1021/pr034020m. [PubMed: 14582645]
- [44]. Sugimoto M, Wong DT, Hirayama A, Soga T, Tomita M. Capillary electrophoresis mass spectrometry-based saliva metabolomics identified oral, breast and pancreatic cancer-specific profiles. *Metabolomics.* 2010;6:78–95. 10.1007/s11306-009-0178-y. [PubMed: 20300169]
- [45]. Eisenhofer G, Prejbisz A, Peitzsch M, Pamporaki C, Masjkur J, Rogowski-Lehmann N, et al. Biochemical diagnosis of chromaffin cell tumors in patients at high and low risk of disease: plasma versus urinary free or deconjugated O-methylated catecholamine metabolites. *Clin Chem.* 2018;64:1646–56. 10.1373/clinchem.2018.291369. [PubMed: 30097498]
- [46]. Ulmer CZ, Yost RA, Chen J, Mathews CE, Garrett TJ. Liquid chromatography-mass spectrometry metabolic and lipidomic sample preparation workflow for suspension-cultured mammalian cells using Jurkat T lymphocyte cells. *J Proteomics Bioinform.* 2015;8:126–32. 10.4172/jpb.1000360. [PubMed: 26401069]

- [47]. Clasquin MF, Melamud E, Rabinowitz JD. LC-MS data processing with MAVEN: a metabolomic analysis and visualization engine. *Curr Protoc Bioinformatics*. 2012 10.1002/0471250953.bi1411s37 Chapter 14:Unit14 1.
- [48]. Adusumilli R, Mallick P. Data conversion with ProteoWizard msConvert. *Methods Mol Biol*. 2017;1550:339–68. 10.1007/978-1-4939-6747-6\_23. [PubMed: 28188540]
- [49]. Chawade A, Alexandersson E, Levander F. Normalyzer: a tool for rapid evaluation of normalization methods for omics data sets. *J Proteome Res*. 2014;13:3114–20. 10.1021/pr401264n. [PubMed: 24766612]
- [50]. <http://bioconductor.org>.
- [51]. McCarthy DJ, Chen YS, Smyth GK. Differential expression analysis of multifactor RNA-Seq experiments with respect to biological variation. *Nucleic Acids Res*. 2012; 40:4288–97. 10.1093/nar/gks042. [PubMed: 22287627]
- [52]. <https://polly.elucidata.io/> PI.
- [53]. Sergushichev AA, Loboda AA, Jha AK, Vincent EE, Driggers EM, Jones RG, et al. GAM: a web-service for integrated transcriptional and metabolic network analysis. *Nucleic Acids Res*. 2016;44:W194–200. 10.1093/nar/gkw266. [PubMed: 27098040]
- [54]. Shannon P, Markiel A, Ozier O, Baliga NS, Wang JT, Ramage D, et al. Cytoscape: a software environment for integrated models of biomolecular interaction networks. *Genome Res*. 2003;13:2498–504. 10.1101/gr.1239303. [PubMed: 14597658]
- [55]. Bergeron RJ, Weimar WR, Luchetta G, Streiff RR, Wiegand J, Perrin J, et al. Metabolism and pharmacokinetics of N1,N11-diethylnorspermine. *Drug Metab Dispos*. 1995;23:1117–25. [PubMed: 8654201]
- [56]. Kuefer R, Hofer MD, Altug V, Zorn C, Genze F, Kunzi-Rapp K, et al. Sodium butyrate and tributyrin induce in vivo growth inhibition and apoptosis in human prostate cancer. *Br J Cancer*. 2004;90:535–41. 10.1038/sj.bjc.6601510. [PubMed: 14735205]
- [57]. Mohanty S, Xu L. Experimental metastasis assay. *J Vis Exp*. 2010 10.3791/1942.
- [58]. Bernacki RJ, Oberman EJ, Seweryniak KE, Atwood A, Bergeron RJ, Porter CW. Preclinical antitumor efficacy of the polyamine analogue N1, N11-diethylnorspermine administered by multiple injection or continuous infusion. *Clin Cancer Res*. 1995;1:847–57. [PubMed: 9816054]
- [59]. Fagerberg L, Hallstrom BM, Oksvold P, Kampf C, Djureinovic D, Odeberg J, et al. Analysis of the human tissue-specific expression by genome-wide integration of transcriptomics and antibody-based proteomics. *Mol Cell Proteomics*. 2014;13:397–406. 10.1074/mcp.M113.035600. [PubMed: 24309898]
- [60]. Richter S, Gieldon L, Pang Y, Peitzsch M, Huynh T, Leton R, et al. Metabolome-guided genomics to identify pathogenic variants in isocitrate dehydrogenase, fumarate hydratase, and succinate dehydrogenase genes in pheochromocytoma and paraganglioma. *Genet Med*. 2019;21:705–17. 10.1038/s41436-018-0106-5. [PubMed: 30050099]
- [61]. Bernacki RJ, Bergeron RJ, Porter CW. Antitumor activity of N,N'-bis(ethyl)spermine homologues against human MALME-3 melanoma xenografts. *Cancer Res*. 1992;52:2424–30. [PubMed: 1568212]
- [62]. Imperiale A, Moussallieh FM, Sebag F, Brunaud L, Barlier A, Elbayed K, et al. A new specific succinate-glutamate metabolomic hallmark in SDHx-related paragangliomas. *PLoS One*. 2013;8:e80539 10.1371/journal.pone.0080539. [PubMed: 24312232]
- [63]. Richter S, Peitzsch M, Rapizzi E, Lenders JW, Qin N, de Cubas AA, et al. Krebs cycle metabolite profiling for identification and stratification of pheochromocytomas/paragangliomas due to succinate dehydrogenase deficiency. *J Clin Endocrinol Metab*. 2014;99:3903–11. 10.1210/jc.2014-2151. [PubMed: 25014000]
- [64]. Gieldon L, William D, Hackmann K, Jahn W, Jahn A, Wagner J, et al. Optimizing genetic workup in pheochromocytoma and paraganglioma by integrating diagnostic and research approaches. *Cancers (Basel)*. 2019;11 10.3390/cancers11060809.
- [65]. Tevosian SG, Ghayee HK. Pheochromocytoma/paraganglioma: a poster child for cancer metabolism. *J Clin Endocrinol Metab*. 2018;103:1779–89. 10.1210/jc.2017-01991. [PubMed: 29409060]

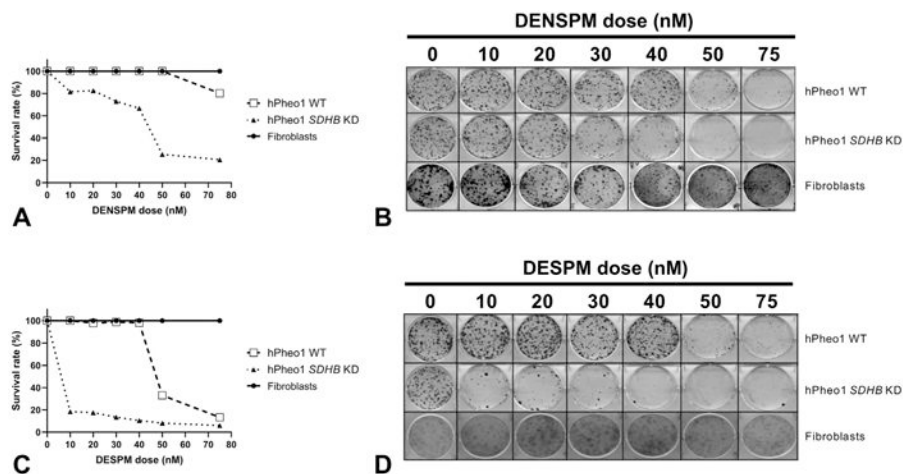
- [66]. Bechmann N, Poser I, Seifert V, Greunke C, Ullrich M, Qin N, et al. Impact of extrinsic and intrinsic hypoxia on catecholamine biosynthesis in absence or presence of Hif2alpha in pheochromocytoma cells. *Cancers (Basel)*. 2019;11 10.3390/cancers11050594.
- [67]. Caron PC, Cote LJ, Kremzner LT. Putrescine, a source of gamma-aminobutyric acid in the adrenal gland of the rat. *Biochem J*. 1988;251:559–62. 10.1042/bj2510559. [PubMed: 3135801]
- [68]. Madsen KK, Larsson OM, Schousboe A. Regulation of excitation by GABA neurotransmission: focus on metabolism and transport. *Results Probl Cell Differ*. 2008;44:201–21. 10.1007/400\_2007\_036. [PubMed: 17579816]
- [69]. Tran L, Fitzpatrick C, Cohn SL, Pytel P. Composite tumor with pheochromocytoma and immature neuroblastoma: report of two cases with cytogenetic analysis and discussion of current terminology. *Virchows Arch*. 2017;471:553–7. 10.1007/s00428-017-2225-9. [PubMed: 28864906]
- [70]. Shida Y, Igawa T, Abe K, Hakariya T, Takehara K, Onita T, et al. Composite pheochromocytoma of the adrenal gland: a case series. *BMC Res Notes*. 2015;8:257 10.1186/s13104-015-1233-6. [PubMed: 26104921]
- [71]. Moon SB. Childhood neuroblastoma masquerading as pheochromocytoma: case report. *Int Med Case Rep J*. 2016;9:65–7. 10.2147/IMCRJ.S100479. [PubMed: 27051319]



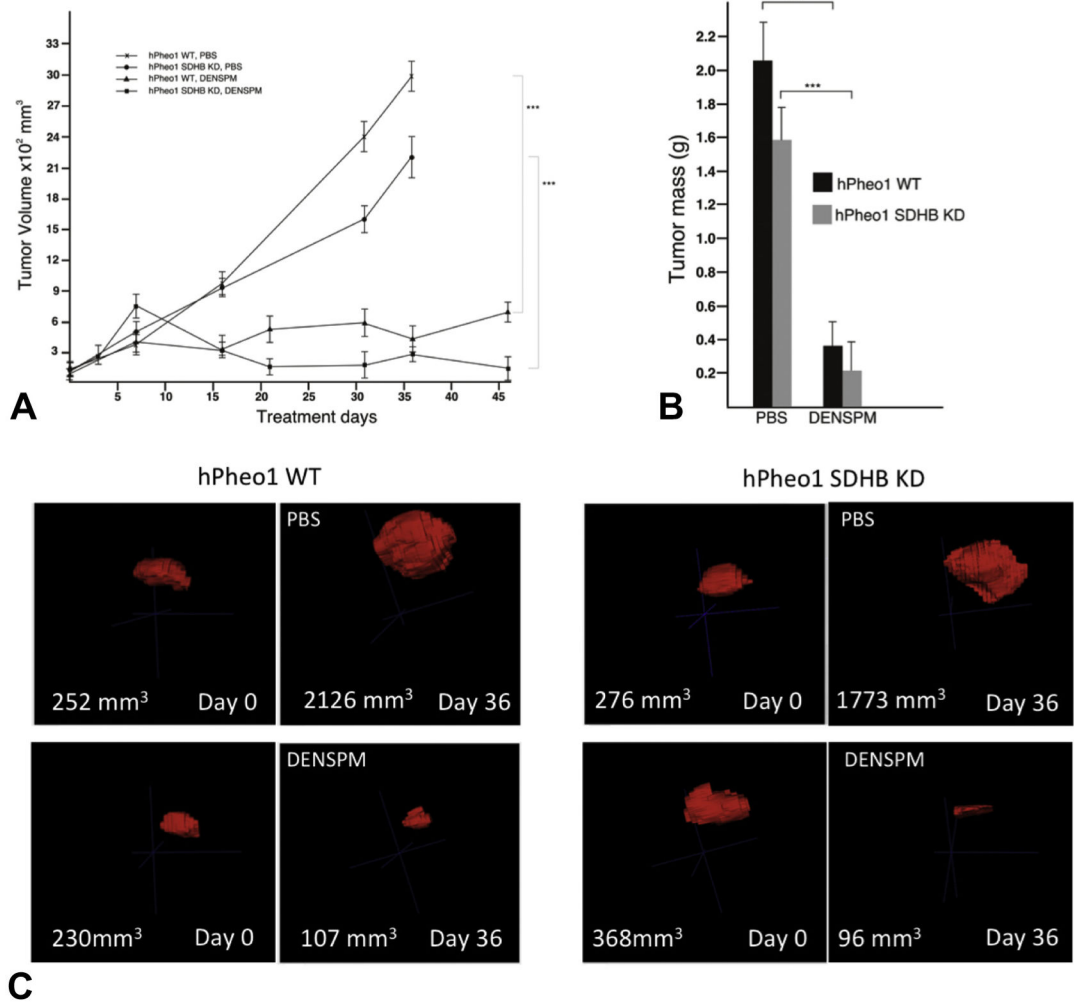
**Fig. 1.** hPheo1 WT and hPheo1 *SDHB* KD cell lines. (a) Quantitative Real Time-PCR analysis in hPheo1 WT (■) and hPheo1 *SDHB* KD (□) are shown; mRNA level were normalized with *GAPDH*. Results show mean  $\pm$  SD,  $n = 3$ . (b) Total-cell extracts were prepared and analyzed by western blot for SDHB protein expression. Note decreased expression of SDHB in both experiments.



**Fig. 2.** Polyamine pathway and altered succinate. Comparison of succinate level in hPheo1 WT and hPheo1 *SDHB* KD are represented on the left and PCC/PGL tumor tissues of non-*SDHx* mutated samples and *SDHx* mutated samples are compared on the right side. Y-axis represents relative intracellular metabolite levels respective to normal samples. Succinate levels are elevated in cells carrying *SDHx* mutation and tumor tissue samples. Significant increases for spermidine and spermine were observed in human *SDHx*-mutated PCC/PGLs; a similar pattern was observed in hPheo1 *SDHB* KD cells, although spermidine did not reach statistical significance in cell line analysis.

**Fig. 3.**

A–D: (A–B). Polyamine analog DENSPM was used for treatment of BJ fibroblasts (....), hPheo1 WT (—) and hPheo1 *SDHB* KD (—) cells at 10 nM–75 nM. (A) The quantitative analysis of the colony-forming assay is represented in left panel. (B) Representative images of colony forming assay for BJ fibroblasts, hPheo1 WT, and hPheo1 *SDHB* KD cells. All experiments were performed in triplicate and represented as mean  $\pm$  SD. (C–D). Polyamine analog DESPM was used for treatment of BJ fibroblasts (....), hPheo1 WT (—) and hPheo1 *SDHB* KD (—) cells at 10 nM–50 nM. (C) The quantitative analysis of the colony-forming assay was represented in left panel. (D) Representative images of colony forming assay for BJ fibroblast, hPheo1 WT, and hPheo1 *SDHB* KD. All experiments were performed in triplicate and represented as mean  $\pm$  SD. Note that DENSPM dose response curves showed IC<sub>50</sub> value for hPheo1WT at 75 nM, whereas hPheo1 *SDHB* KD showed a response at 40 nM (3B). Also note that BJ fibroblasts showed no sensitivity towards DENSPM at this concentration range (3B). For DESPM, the dose response data demonstrated a very low IC<sub>50</sub> for hPheo1 *SDHB* KD at 10 nM, whereas hPheo1 WT showed an IC<sub>50</sub> of 50 nM (3C and 3D).

**Fig. 4.**

A–C. DENSPM treatment in hPheo1 WT and hPheo1 *SDHB* KD xenograft models. (A) Four cohorts of male mice (Taconic C.B-Igh-1b/IcrTac-Prkdcscid;  $n = 6–10$  per cohort) were administered vehicle control (PBS) or DENSPM (60 mg/kg) via i.p. injection, daily over 6 weeks to generate tumor growth curves of cell line xenografts. Tumor volumes are displayed as means  $\pm$  SD (\*\* $p < .001$ ). (B) Weights of tumors isolated at endpoint after 45 days of treatment. Tumor weights are displayed as means  $\pm$  SD (\*\* $p < .001$ ). (C) Representative three-dimensional images of the tumors obtained through MRI volumetric analysis in four animal cohorts as indicated, before and after treatment with either PBS or DENSPM. Note that DENSPM administration resulted in a reduction of tumor volume, with tumor growth inhibition (TGI) reaching 75% and 86% in hPheo1 WT and hPheo1 *SDHB* KD cohorts, respectively. DENSPM significantly reduced tumor volume, with a TGI of ~66% in both cohorts by day 16. Tumor weight in treated animals was also significantly reduced compared to vehicle-injected mice (4B).

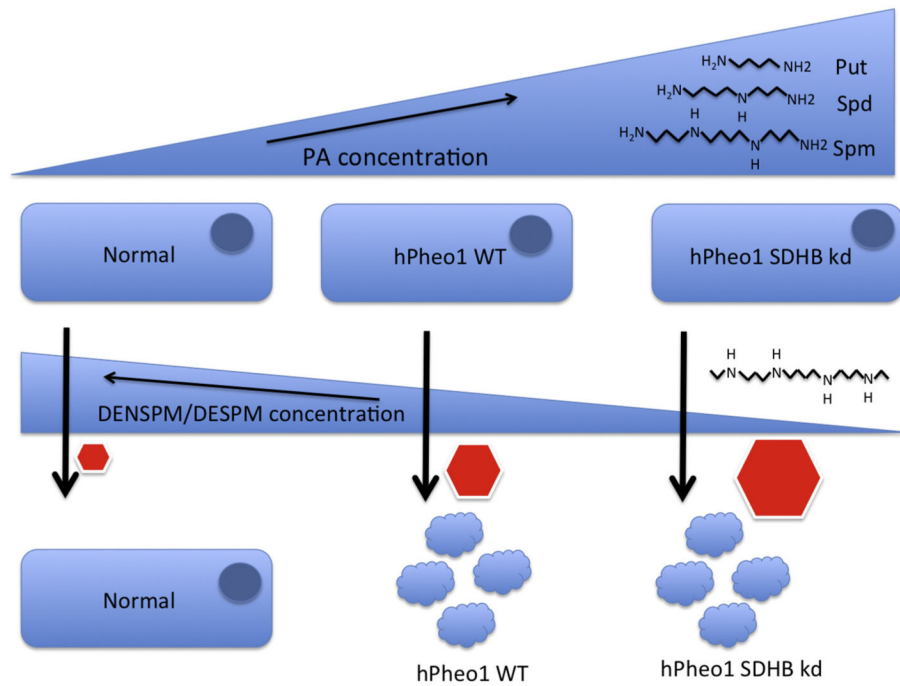


**Fig. 5.** Graphic summary of key results. Polyamine (PA) pathway is overactive in cells carrying SDHB mutations and in PCC/PGL *SDHx*-mutated tumor tissue samples. Treatment with polyamine pathway inhibitors preferentially suppresses growth of hPheo1 *SDHB* KD and hPheo1 WT compared to control cells in culture and in a mouse xenograft model.